Simplified Detection Techniques for Serially Concatenated Coded Continuous Phase Modulations

C2007
Dileep Kumaraswamy

Submitted to the Department of Electrical Engineering and Computer Science and the Faculty of the Graduate School of the University of Kansas in partial fulfillment of the requirements for the degree of Master's of Science

Thesis Committee:

Dr. Erik Perrins (Chair)

Dr. Victor Frost

Dr. Shannon Blunt

6^{th} July, 2007

Date of Thesis Defense

The Thesis Committee for Dileep Kumaraswamy certifies
that this is the approved version of the following thesis:

Simplified Detection Techniques for Serially Concatenated Coded Continuous Phase Modulations

Thesis Committee:

Dr. Erik Perrins (Chair)

Dr. Victor Frost

Dr. Shannon Blunt

6^{th} July, 2007

Date Approved

Simplified Detection Techniques for Serially Concatenated Coded Continuous Phase Modulations

Dileep Kumaraswamy
Master of Science in Electrical Engineering
University of Kansas

Abstract

Serially concatenated coded (SCC) systems with continuous phase modulations (CPMs) as recursive inner codes have been known to give very high coding gains at low operative signal to noise ratios (SNRs). Moreover, concatenated coded systems with iterative decoding approach the bit error rate bounds given by the maximum likelihood criterion at a lesser complexity. However, when highly bandwidth efficient CPMs are used, they pose two fundamental problems — extremely high decoding complexity and carrier phase synchronization. Desirable properties of SCC systems and their subsequent applications to deep space communication has renewed research interests to look for possible solutions to the above problems. Several complexity reduction techniques have been surveyed in this thesis to address the problem of efficient detection at *low* SNR operation of the SCC systems. Perfect synchronization at the receiver is often times a delusive assumption. This makes non-coherent detection an attractive option. A heuristic and practical non-coherent detection algorithm is proposed for moderate phase noise environments, which result in huge savings in complexity compared to the available algorithms for non-coherent detection.

To

my uncle Prabhu (Mama)

and

my aunt Usha (Ammami)

Acknowledgements

I always find myself short of words to express my sincere most gratitude to my uncle Dr. M.S.S Prabhu (Prabhu Mama) and my aunt Usha Prabhu (Usha Ammami). They have mentored me and cared for me since my childhood. They have been rock solid in their support to me during good and bad times. I have learnt from them some of the most important values in life. Without their blessings, I could never have been where I am now. They have always been my best friends and role models and I hope I live up to their expectations in the coming years.

I would like to thank Prof. Erik Perrins for giving me an opportunity to work with him. His advice and feedback were invaluable to me. Being his first graduate student makes me feel very special. I would like to thank Kanagaraj for his work on the error control coding part of the project. I would also like to thank the Test Resource Management Center (TRMC) Test and Evaluation/Science and Technology (T&E/S&T) Program for their support. This work was funded by the T&E/S&T Program through the White Sands Contracting Office, contract number W9124Q-06-P-0337.

I would like to thank Prof. Victor Frost for being on my committee. I would also like to express my thanks to Prof. Shannon Blunt. Classes taught by him helped me develop greater interest in DSP. My special thanks to Prof. Alexander Wyglinski, for his advice and also inputs on technical writing.

I would like to thank Raveesh, my childhood friend and companion whose friendship has given me immense happiness. I would like to thank my sister Yamuna, parents and relatives who have supported me. I can never forget to say thanks to all my friends who have helped me and have always been an inseparable part of my life. Especially, I would like to thank Kiran, Manjunath, Vishal, Deepthi, Shruthi and others who have made my stay in Lawrence and experience at KU, extremely memorable.

Page intentionally left blank

Contents

List of Figures

List of Tables

Chapter 1

Introduction

Digital modulation is the process of converting a digital information bit stream or code words from the source encoder into functions of time by varying (modulating) the parameters of waveforms such as amplitude, frequency and phase. The aim of a digital communication system is to transmit information reliably, being judiciously conservative in the usage of valuable resources at hand such as bandwidth, power and processing power (handling computational complexity). In order to achieve this, the chosen modulation scheme should match the channel characteristics. Prior to the 1980's, modulation and coding were treated with different abstraction levels, studied and researched independent of the other to achieve high performance. The first attempt to combine principles of modulation and coding was done in 1982. Gottfried Ungerboeck, in his landmark paper [1] showed that one could achieve very high coding gains by signal set partitioning to achieve improved Euclidean distance. The invention of parallel concatenated coding schemes in turbo codes in 1993 by Berrou, Glavieux and Thitimajshima [2], propelled a tremendous amount of research towards achieving coding gains to reach the Shannon's limit. Since then, a new area of research has focussed on serial concatenation of modulation with error control coding, which derives its motivation

from the principles of turbo codes. The block diagram of a simple digital communication system in Fig. 1.1, indicates modulation and coding to be a combined area of study, which is the *crux* of this thesis.

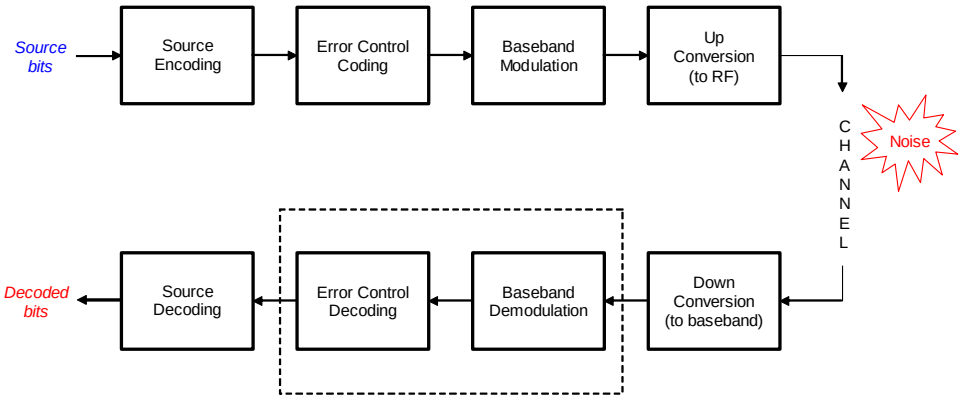

Figure 1.1. A Simple Digital Communication System.

Continuous phase modulation (CPM) belongs to the class of *non-linear* digital modulation schemes with *memory*.[1] CPM signals are endowed with several desirable properties such as high detection efficiency and high spectral efficiency. The constant envelope property of the CPM waveforms give amplifiers high *power efficiency*. CPMs can be operated with non-linear power amplifiers. They are also suitable for communication over *non-linear* channels which may destroy amplitude relationships. Examples of non-linear channels are mobile and satellite channels which have a time-varying channel response (fading). On the other hand, modulations such as pulse amplitude modulation (PAM) and quadrature amplitude multiplexing (QAM) show performance deterioration due to *distortion* of the signal constellation, when passed through a non-linear power amplifier. In *phase shift keying* (PSK), the phase of the signal containing the information is obtained by a simple *mapping* of the input symbol to a *defined* signal

[1] A modulation is said to have memory if the signal (modulated waveform) in any symbol interval depends on the symbols transmitted during the previous symbol intervals.

constellation point. The PSK signal can take on finite (discrete) values of phase. Likewise, the information in a CPM signal is also contained in its phase. However, CPM is *different* from PSK because the phase of the CPM is *continuous* and at any time is a *relative* quantity with respect to the input symbol at that time. In other words, an input symbol is *not tied* to any constellation point. This comes from the fact that CPM is a modulation with memory.

Owing to the several properties described, CPMs are used in deep space communication [3], wireless modems, 802.11 FHSS and Bluetooth [4]. The European standard for personal communication system (PCS) *global system for mobile communications* (GSM) uses *Gaussian minimum shift keying* (GMSK), which belongs to the class of CPMs.

1.1 Signal Representation for CPM

The signal representation for a complex baseband CPM is of the form

$$s(t;\boldsymbol{\alpha}) = e^{j\phi(t;\boldsymbol{\alpha})}, \tag{1.1}$$

where $\phi(t;\boldsymbol{\alpha})$ represents the phase of the CPM given by the linear filtering of information bits/codewords. In the most generic form [5], we have

$$\phi(t;\boldsymbol{\alpha}) = 2\pi \sum_{i=-\infty}^{\infty} h_{\underline{i}}\alpha_i q(t-iT_s), \qquad nT_s \leq t \leq (n+1)T_s, \tag{1.2}$$

where the phase of the CPM is *constrained* to be continuous by the use of a phase pulse $q(t)$ which defines the *phase trajectory* due to an input symbol,[2] $h_{\underline{i}}$ is the *modulation index* associated with the symbol α_i in the i-th symbol interval and T_s is the symbol

[2] An impulse frequency pulse does not have memory and results in regular PSK.

duration. The modulation index changes cyclically through a finite set of N_h modulation indices ($\underline{i} \triangleq i \bmod N_h$). The *value* of the modulation indices indicate the amount of phase change introduced at the occurrence of a symbol. If there is more than one modulation index, then the CPM is called as a multi-h CPM. The source alphabet can be binary where $\alpha \in \{-1, +1\}$, quaternary where $\alpha \in \{-3, -1, +1, +3\}$, octal where $\alpha \in \{-7, -5, \ldots, +5, +7\}$, etc. Further, the *phase pulse* $q(t)$ can be viewed as the time integral of the frequency pulse whose area equals $\frac{1}{2}$, given by

$$q(t) = \begin{cases} 0, & t \leq 0 \\ \displaystyle\int_0^t g(\tau)\, d\tau, & 0 \leq t \leq LT_s \\ \frac{1}{2}, & t \geq LT_s, \end{cases} \tag{1.3}$$

where $g(t)$ is the *frequency pulse* of duration LT_s. Since the area of $q(t)$ is now fixed to be $\frac{1}{2}$, the amount of phase change for a CPM depends *only* on the modulation index.

The shape of the frequency pulse is an important parameter which determines the spectral properties of the CPM. Some of the commonly used pulse shapes are the length-L rectangular (LREC) pulse and the length-L raised cosine (LRC) pulse. The telemetry group (TG) standard shaped offset QPSK (SOQPSK) uses a TG standard frequency pulse. An example of a 3RC pulse is shown in Fig. 1.2. The LREC and LRC pulses are defined by Eq. (1.4) and Eq. (1.5) respectively,

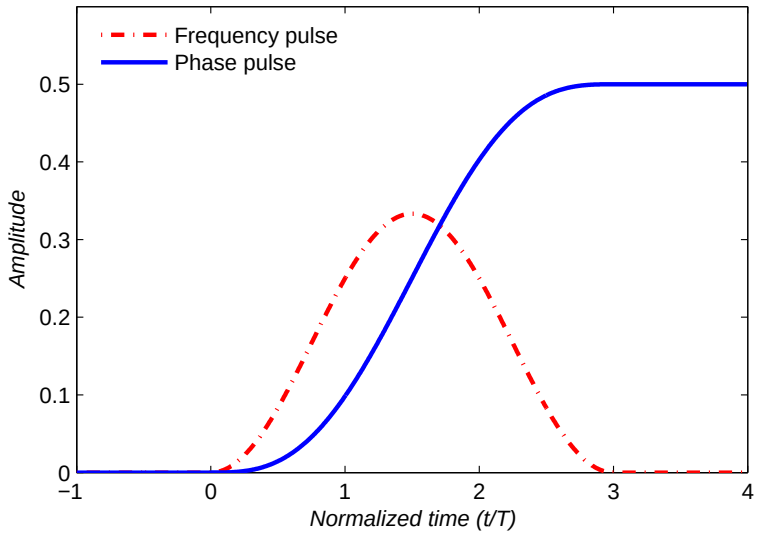

Figure 1.2. A 3RC Frequency Pulse.

$$g(t) = \begin{cases} \frac{1}{2LT_s}, & 0 \le t \le LT_s \\ 0, & \text{otherwise,} \end{cases} \tag{1.4}$$

$$g(t) = \begin{cases} \frac{1}{2LT_s}\left[1 - \cos\left(\frac{2\pi t}{LT_s}\right)\right], & 0 \le t \le LT_s \\ 0, & \text{otherwise.} \end{cases} \tag{1.5}$$

Due to the constraints on the *causal* phase pulse $q(t)$ in Eq. (1.3), Eq. (1.2) can be written as

$$\phi(t;\boldsymbol{\alpha}) = \underbrace{\pi \sum_{i=0}^{n-L} h_{\underline{i}}\alpha_i}_{\vartheta_{n-L}} + \underbrace{2\pi \sum_{i=n-L+1}^{n} h_{\underline{i}}\alpha_i q(t - iT_s)}_{\theta(t)}, \qquad nT_s \le t \le (n+1)T_s. \tag{1.6}$$

The L-tuple *correlative state vector*

$$\boldsymbol{\alpha}_n = \alpha_{n-L+1}, \ldots, \alpha_n, \tag{1.7}$$

in $\theta(t)$ contains the L most recent symbols modulated by the *time-varying* part of the phase pulse $q(t)$, which contribute to the phase trajectory of the CPM in the current signaling interval. The state of a CPM is specified by

$$\sigma' = \left[\vartheta_{n-L}, \alpha_{n-L+1}, \ldots, \alpha_{n-1}\right]. \tag{1.8}$$

On the assumption that the modulation index is a *rational* quantity [5], we can write

$$h_{\underline{i}} = \frac{2K_{\underline{i}}}{P'}, \tag{1.9}$$

where $K_{\underline{i}}$ and P' are relatively prime. The *cumulative phase* ϑ_{n-L} in Eq. (1.6) now becomes

$$\vartheta_{n-L} = \frac{2\pi}{P'} \sum_{i=0}^{n-L} K_{\underline{i}} \alpha_i, \tag{1.10}$$

which can take on P' distinct values when taken *modulo*-2π (property of the complex phase). The cumulative phase ϑ_{n-L} is the the phase of the CPM at the beginning of the symbol interval (at the current time n), into which symbols older than L symbol times have been absorbed and the P' distinct values of the cumulative phase are given by $\vartheta_{n-L} \in \left\{\frac{0\cdot 2\pi}{P'}, \frac{1\cdot 2\pi}{P'}, \frac{2\cdot 2\pi}{P'}, \ldots, \frac{(P'-1)\cdot 2\pi}{P'}\right\}$. Finite number of values of the cumulative phase resulting from the assumption of a rational modulation index gives the CPM a finite state representation (trellis) given by Eq. (1.8). This is desirable since the complexity of the decoding algorithm is proportional to the state complexity of the CPM. The details of the algorithm used are described in the Chapter 2.

All the possible phase trajectories in a CPM can be represented by by a phase cylinder, which is helpful in visualizing the phase changes in a CPM. The phase cylinders for *minimum shift keying* (MSK) and *pulse code modulation/frequency modulation* are shown in Fig. 1.3 and Fig. 1.4 respectively. $P' = 4$ values of cumulative phase ϑ_{n-L}

in MSK result from a modulation index of $h = \frac{1}{2}$. In PCM/FM, the cumulative phase ϑ_{n-L} takes on 20 values resulting from $h = \frac{7}{10}$.

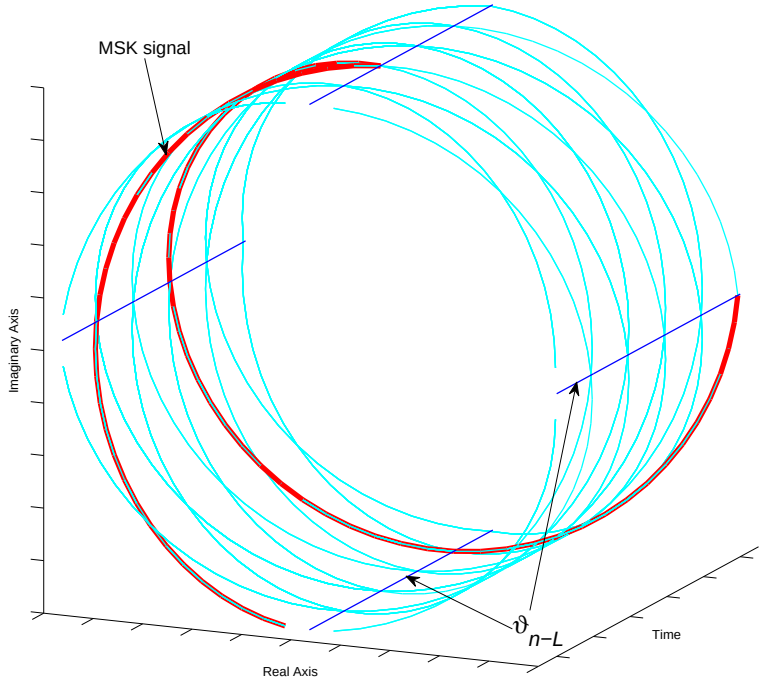

Figure 1.3. Phase Cylinder for MSK.

1.2 The Telemetry Standard CPMs

The aeronautical telemetry standard IRIG 106-04 has been developed by range commanders council (RCC) to serve the technical needs of the department of defense (DOD). Among the many CPMs (resulting from combinations of h, M, L, pulse shape, mapping rule, etc), some of them have gained popularity driven by the needs of the application, such as spectral efficiency, power efficiency and decoding complexity. Three

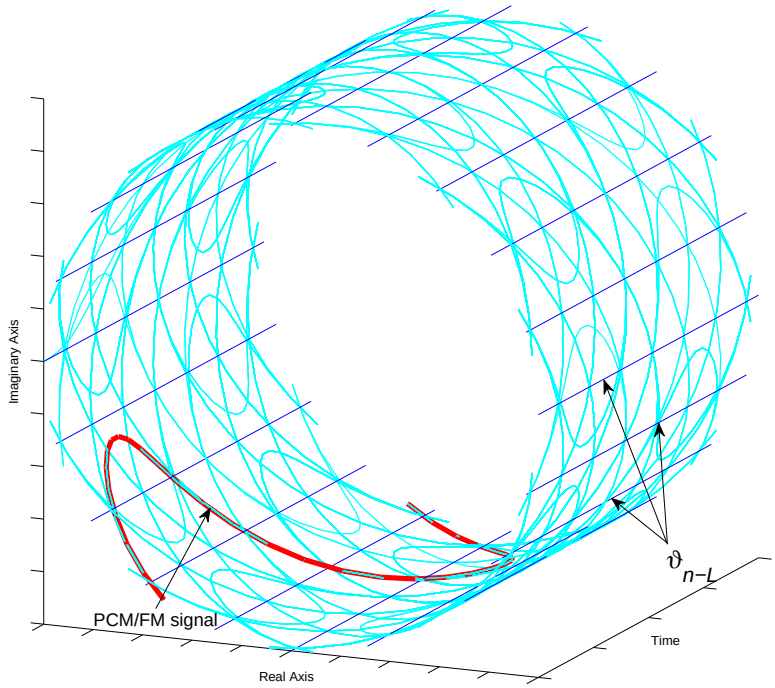

Figure 1.4. Phase Cylinder for PCM/FM.

popular modulation schemes (three tiers of bandwidth efficiency), each with unique properties, have been developed by the aeronautical telemetry to operate in the UHF carrier frequencies.

1.2.1 PCM/FM (Tier-0)

Pulse code modulation/frequency modulation (PCM/FM) has been used in the aeronautical telemetry standard since 1970's. PCM/FM is a binary CPM specified by the CPM parameters $h = \frac{7}{10}$, $M = 2$, 2RC. It has a moderate decoding complexity. It is the least spectrum efficient, but the most detection efficient among the three modulations considered. It is also least sensitive to phase noise and consequently the easiest to

synchronize.

1.2.2 SOQPSK-TG (Tier-1)

In offset quadrature shift keying (OQPSK), the half symbol time delay in the *quadrature phase* data stream w.r.t the *in phase* data stream aids in avoiding the instantaneous 180° phase shifts. OQPSK also has improved power spectrum compared to QPSK. However, it still does not avoid the waveform envelope fluctuations due to the instantaneous transitions between adjacent phase states. Shaped offset quadrature phase shift keying (SOQPSK) is often referred to be derivative of OQPSK and MSK. At the cost of detection efficiency, it is spectrally more efficient than OQPSK/MSK.

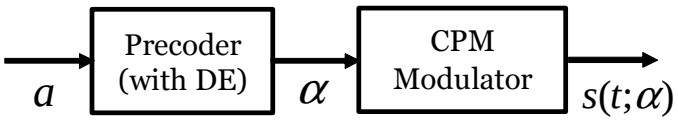

Figure 1.5. Precoding in SOQPSK.

SOQPSK uses a precoder to convert binary information to ternary symbols. The ternary symbols are modulated by a CPM modulator (MSK modulator, $h = \frac{1}{2}$). While the use of precoder (see Fig. 1.5) imposes OQPSK like properties, the use of frequency pulse gives SOQPSK a constant envelope like in a CPM. It is interesting to note that from the CPM stand point, SOQPSK is not a quadrature signalling scheme, but a *binary* signalling scheme, modulated using *ternary* symbols $\alpha \in \{-1, 0, +1\}$. Although the modulating symbols are ternary, in any signaling interval, they assume only 2 values $\in \{-1, 0\}$ or $\{+1, 0\}$. Therefore, the bandwidth efficiency is $m = \log_2(M) = 1$ bit/symbol

as in a binary scheme.[3]

The ternary symbol sequence has special properties introduced by the precoder [6] defined by

$$d_n = a_n \oplus d_{n-2}, \tag{1.11}$$

$$\alpha_n = (-1)^n a_n d'_{n-1} d'_{n-2}, \tag{1.12}$$

where d'_n is an antipodal version of d_n and is given by $d'_n = 2d'_n - 1$. $a_n \in \{0, 1\}$ is the data bit at time n. The state variables a_{n-1} and a_{n-2} are ordered to ensure that the inphase bit is always the most significant bit (MSB) and the quadrature phase bit is always the least significant bit (LSB). Hence the data bits d_{n-2}, d_{n-1} represent the state of the *double differentially encoded* SOQPSK (DSOQPSK) at even symbol times and the data bits d_{n-1}, d_{n-2} represent the state at odd symbol times [7]. The precoder imposes the following constraints on the ternary data —

1. At any symbol interval, $\alpha_n \in \{0, +1\}$ or $\{0, -1\}$.

2. Whenever $\alpha_n = 0$, the precoded binary alphabet for α_{n+1} changes from the one used for α_n, otherwise it does not.

3. α_n cannot directly change -1 to $+1$ and viceversa, in *successive* symbol intervals *i.e.,* a $+1$ can be followed by a $+1$ or 0 but not -1 and similarly a -1 can be followed by a -1 or 0 but not $+1$. This introduces correlation to the ternary symbols and gives SOQPSK a *more compact bandwidth* compared to MSK/OQPSK.

The *time-varying trellis* of the SOQPSK-MIL which uses a 1REC frequency pulse (just like MSK) is given in Fig. 1.6, which indicates the relation between the input and

[3] In the literature, SOQPSK is also represented as having $h = \frac{1}{4}$ and ternary symbols $\alpha \in \{-2, 0, +2\}$. However, they both give the same phase change $h\pi\alpha$ at the occurrence of a symbol.

the precoded bits. [4] The use of a *recursive* precoder (which incorporates differential encoding) is *necessary* for both SCC systems and non-coherent detection.

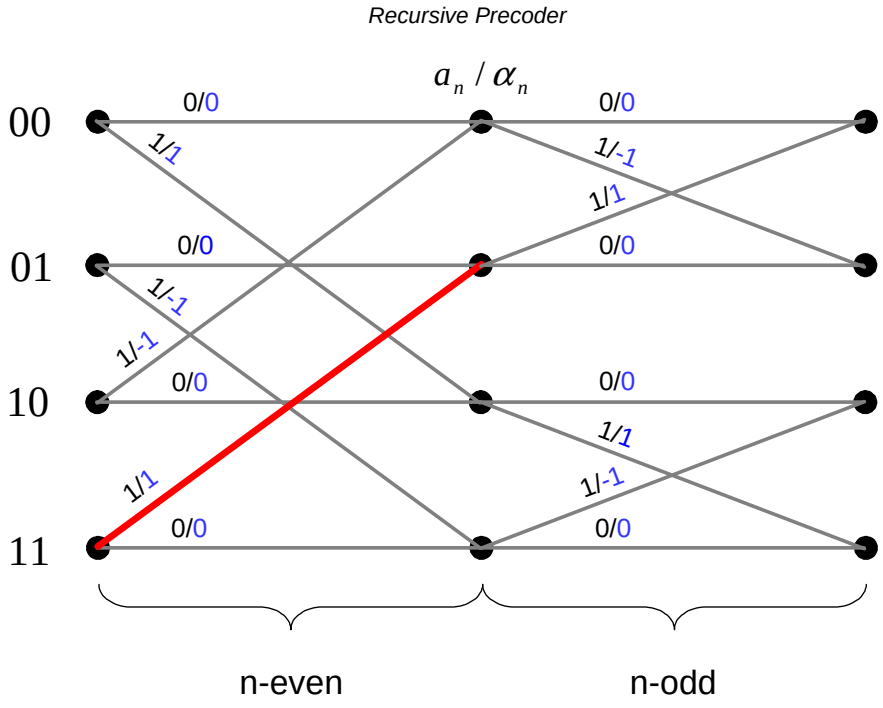

Figure 1.6. SOQPSK-MIL Trellis.

Another aspect in the decoding of SOQPSK as a CPM lies in the mapping of the trellis states of SOQPSK onto CPM phase states. For this purpose we use the mapping given in Fig. 1.7 to use the SISO decoding algorithm in Chapter 2.

The SOQPSK-TG is uses a TG standard phase pulse which is 8 symbols long. This means, the state complexity for SOQPSK-TG given by Eq. (1.8) is 512 states while the state complexity for SOQPSK-MIL is 4. The SOQPSK-TG frequency in Fig. 1.8, is

[4] A trellis completely describes the states and phase changes in the CPM.

State	P_l
00	3
01	2
10	0
11	1

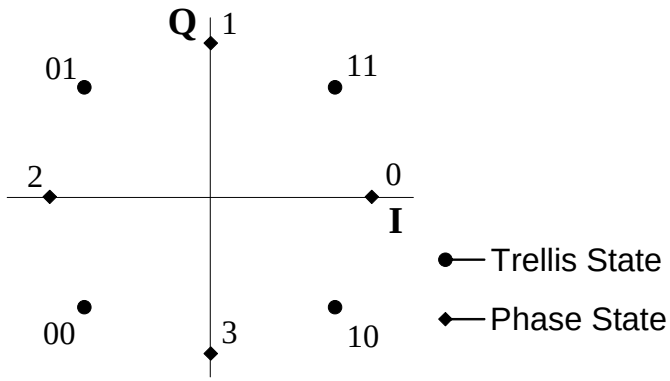

Figure 1.7. Mapping of SOQPSK Trellis States onto MSK Phase States.

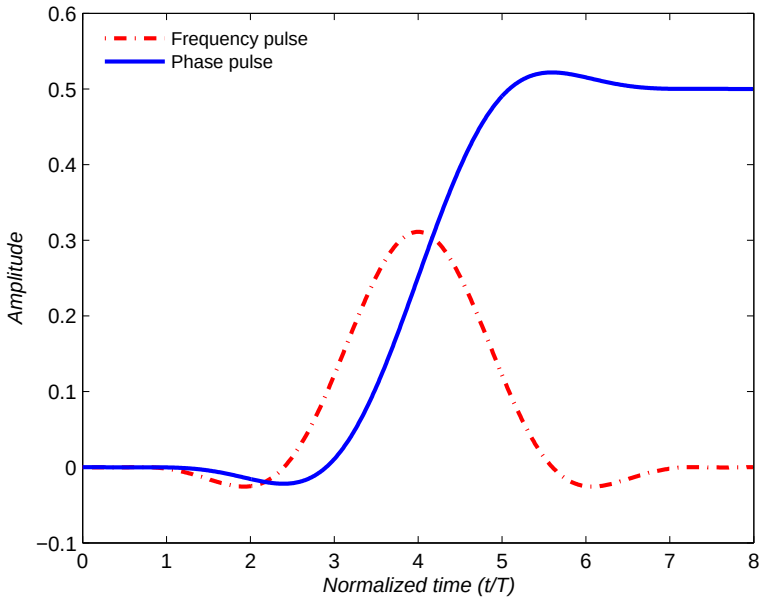

Figure 1.8. SOQPSK-TG: Frequency and Phase Pulses.

given by

$$f_{\text{TG}}(t) = A\frac{\cos\left(\frac{\pi\rho Bt}{2T_s}\right)}{1-4\left(\frac{\rho Bt}{2T_s}\right)^2} \times \frac{\sin\left(\frac{\pi Bt}{2T_s}\right)}{\frac{\pi Bt}{2T_s}} \times w(t), \tag{1.13}$$

where the window is defined by

$$w(t) = \begin{cases} 1, & 0 \leq \left|\frac{t}{2T_b}\right| \leq T_1 \\ \frac{1}{2}+\frac{1}{2}\cos\left(\frac{\pi}{T_2}\left(\frac{t}{2T_b}-T_1\right)\right), & T_1 \leq \left|\frac{t}{2T_b}\right| \leq T_1+T_2 \\ 0, & T_1+T_2 < \left|\frac{t}{2T_b}\right|. \end{cases}$$

The normalization constant A is chosen to give the pulse an area of $\frac{1}{2}$, $T_1 = 1.5$, $T_2 = 0.5$, $\rho = 0.7$, and $B = 1.25$. The SOQPSK-TG has the least decoding complexity (with the pulse truncation technique), of all the three modulations considered and is moderately sensitive to phase noise.

1.2.3 ARTM CPM (Tier-2)

The advanced range telemetry (ARTM) CPM is a quaternary multi-h CPM specified by the parameters $h = \{\frac{4}{16}, \frac{5}{16}\}$, $M = 4$, 3RC. In single-h CPMs, while higher M improves the bandwidth efficiency, it reduces the power efficiency. Interestingly, the use of alternating modulation indices improve the *distance* associated with the error events and thus also improve the detection efficiency, shown in Fig. 1.9. As one would anticipate, the gain in ARTM CPM comes at a cost of a 4 fold increase in complexity compared to the single-h CPM with $h = \frac{1}{4}$. The ARTM CPM has the highest decoding complexity and the least power efficiency among all the three modulations, but has the best spectral efficiency. This reduces the required carrier spacing in applications with limited available bandwidth.

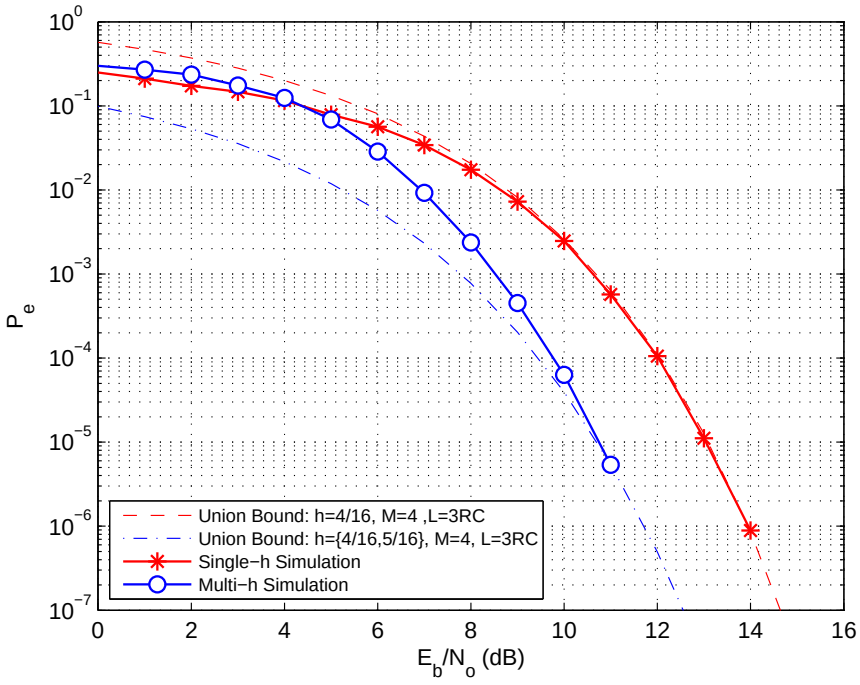

Figure 1.9. Coding Gain in Multi-h CPMs.

1.3 Previous Work and Motivation for the Thesis

Serially Concatenated Coding (SCC) schemes give high class performance in spectral and power efficiencies but trade-off very badly with implementation complexity. A qualitative analysis of SCC CPM schemes has been done in [8]. Optimal decoding, which approaches the union bounds defined by the maximum likelihood (ML) decoding, is often times impractical and unaffordable to be used in digital hardware implementation, where there is often times a shortage of computing power. Bandwidth efficient CPMs in particular, have large decoding complexity and are hard to synchronize. Consequently, there is a drain of computational resources in an effort to do optimal decoding. Previous works on reducing decoding complexity have not been applied to SCC systems [8, 9]. A technique called frequency pulse truncation applied to SCC

SOQPSK-TG, reported a complexity reduction by a factor of 128 with a performance loss of just 0.2 dB [6]. This is a motivation to look for complexity reduction techniques applicable to other systems such as SCC PCM/FM. Previously reported non-coherent detection schemes use extremely complex metric computations [10] and cannot be effectively implemented in digital hardware. Hence non-coherent detection is considered with special interest. In this thesis, some simplified detection schemes are presented applicable to SCC systems. A summary of the thesis work is given below:

- A SCC system using PCM/FM is developed for the first time.
- Simplified detectors using decision feedback and pulse truncation technique are presented for SCC PCM/FM, which give a performance close to the optimal detection but with less than half the complexity of optimal decoding.
- A simple heuristic non-coherent algorithm is presented, which is applicable to SCC CPMs. Using this algorithm, non-coherent detectors have been developed for uncoded PCM/FM, SOQPSK-MIL, reduced complexity SOQPSK-TG (reduced complexity SOQPSK-TG is presented in [6]) and ARTM CPM. Also, presented here are non-coherent detectors for the SCC reduced complexity SOQPSK-TG and SCC PCM/FM. The algorithm presented allows recovery of information in presence of moderate *phase noise*, and achieves close to optimal coherent detection without a significant increase in needed signal power (less than a fraction of a decibel in most cases).
- The proposed non-coherent algorithm is also applied to the reduced complexity detector for SCC PCM/FM and uncoded ARTM . Several numerical results are presented. Among them, a *half* complexity non-coherent detector for SCC PCM/FM and a non-coherent detector for uncoded ARTM CPM with one-sixteenth

complexity, both in comparison to optimal state decoding, are the *key contributions* of this thesis.

1.4 Thesis Outline

In this thesis, the contents have been organized as follows. *Chapter* 2 deals with the *soft-input soft-output* (SISO) algorithm, metric computations used in decoding algorithms and also provides an overview of SCC systems. *Chapter* 3 explains the available reduced complexity techniques which are applied to CPMs in SCC systems. *Chapter* 4 presents the non-coherent detection algorithm, which is applicable to both uncoded and SCC systems. The simulation results with explainations are presented in *Chapter* 5. The conclusions and a vision for future work are offered in *Chapter* 6.

1.5 Paper Publication

This thesis is partly based on the following publication:

Dileep Kumaraswamy and Erik Perrins, "On Reduced Complexity Techniques For Bandwidth Efficient Continuous Phase Modulations in Serially Concatenated Coded Systems", to appear in Proceedings of the International Telemetering Conference (ITC), Las Vegas, NV, October 22-25, 2007.

Chapter 2

System Description

2.1 Maximum Likelihood Decoding of CPM

The complex baseband noisy signal at the receiver is

$$r(t) = s(t; \boldsymbol{\alpha}) + n(t), \tag{2.1}$$

where $n(t)$ is complex-valued additive white Gaussian noise (AWGN) with double-sided power spectral density $\frac{N_0}{2}$. A channel with white noise has an autocorrelation which is almost an an impulse function, which means it does not have memory and affects transmitted symbols independently. Further, dependent bit errors in case of a CPM are *only* due to the memory of the CPM. Based on the AWGN assumption of noise, the receiver tries to optimize the *log-likelihood* function[1] for optimal detection of underlying hypothesized information sequence $\widetilde{\boldsymbol{\alpha}}$, which is [5]

$$L(\widetilde{\boldsymbol{\alpha}}) \sim -\int_{-\infty}^{\infty} |r(t) - s(t; \widetilde{\boldsymbol{\alpha}})|^2 dt. \tag{2.2}$$

[1]Log-likelihood functions spell out probabilities for possible outcomes of $\widetilde{\alpha}$

Due to the constant envelope property of CPMs, maximizing Eq. (2.2) is equivalent to maximizing the correlation between the received signal and the transmitted signal

$$\lambda(\widetilde{\boldsymbol{\alpha}}) = \mathrm{Re}\left\{\int_{-\infty}^{\infty} r(t)s^*(t;\widetilde{\boldsymbol{\alpha}})dt\right\}. \tag{2.3}$$

The correlation up to the current symbol interval is

$$\lambda_n(\widetilde{\boldsymbol{\alpha}}) = \mathrm{Re}\left\{\int_{-\infty}^{(n+1)T_s} r(t)s^*(t;\widetilde{\boldsymbol{\alpha}})dt\right\}, \tag{2.4}$$

which can be *recursively* expanded into

$$\lambda_n(\widetilde{\boldsymbol{\alpha}}) = \lambda_{n-1}(\widetilde{\boldsymbol{\alpha}}) + \mathrm{Re}\left\{\int_{nT_s}^{(n+1)T_s} r(t)s^*(t;\widetilde{\boldsymbol{\alpha}})dt\right\}, \tag{2.5}$$

where a *forward* incremental metric is computed. We have broadly two (trellis based) options to implement the recursive ML decoding—

1) The Viterbi algorithm (VA) — which performs *maximum likely sequence detection* (MLSD) of the underlying information $\widetilde{\boldsymbol{\alpha}}$ using a forward recursion over a block of data to minimize the word (sequence) error rate.

2) The soft-input soft-output (SISO) algorithm — which minimizes the symbol error rate of the underlying information $\widetilde{\boldsymbol{\alpha}}$ using a forward and a reverse recursion over a block of data and is more complex than the VA. The SISO algorithm is a derivative of the popular *Bahl Cocke Jelenik Raviv* (BCJR) algorithm [11].

Since the focus of the research is on *serial concatenation* of CPMs with convolutional codes (CCs), the SISO algorithm for CPM[2] is discussed in the following section.

[2]The SISO algorithm is applicable to both CPMs and CCs, but the focus of the work being on CPMs, the SISO algorithm for CCs is not discussed.

2.2 Matched Filtering and SISO Algorithm for CPM

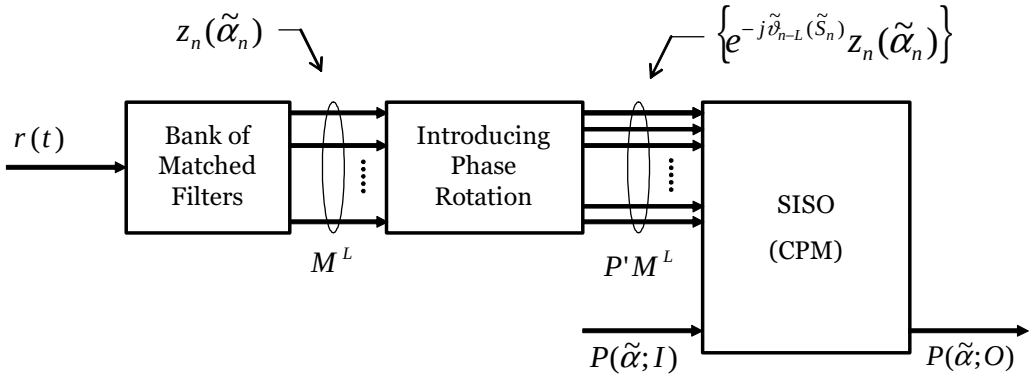

Figure 2.1. Matched Filtering for the ML decoding of CPM.

Modulations with memory such as CPMs, can be represented by a trellis which completely describe the states and phase changes in a CPM. The trellis for MSK is shown in Fig. 2.2. Each branch of the trellis is completely specified by the state σ' and the current branch symbol α_n. So, from Eq. (1.8), we see that the number of states in the trellis is $P' \times M^{L-1}$ from the P' cumulative phases and M^{L-1} symbol combinations resulting from the $L-1$ tuple. Since each state is associated with M possible branch symbols, the number of branches is $P'M^L$. A *bank of matched filters* is used implement the ML decoding in Eq. (2.5). Matched filters are nothing but time-reversed complex-conjugated reference waveforms. The branch metrics for the trellis based SISO algorithm are obtained by a set of M^L matched filtered outputs combined with P' cumulative phases as shown in Fig. 2.1 and are given by

$$\digamma_n(\widetilde{S}_n, \widetilde{E}_n) = \mathrm{Re}\left\{e^{-j\tilde{\vartheta}_{n-L}(\widetilde{S}_n)} z_n(\widetilde{\boldsymbol{\alpha}}_n)\right\}, \tag{2.6}$$

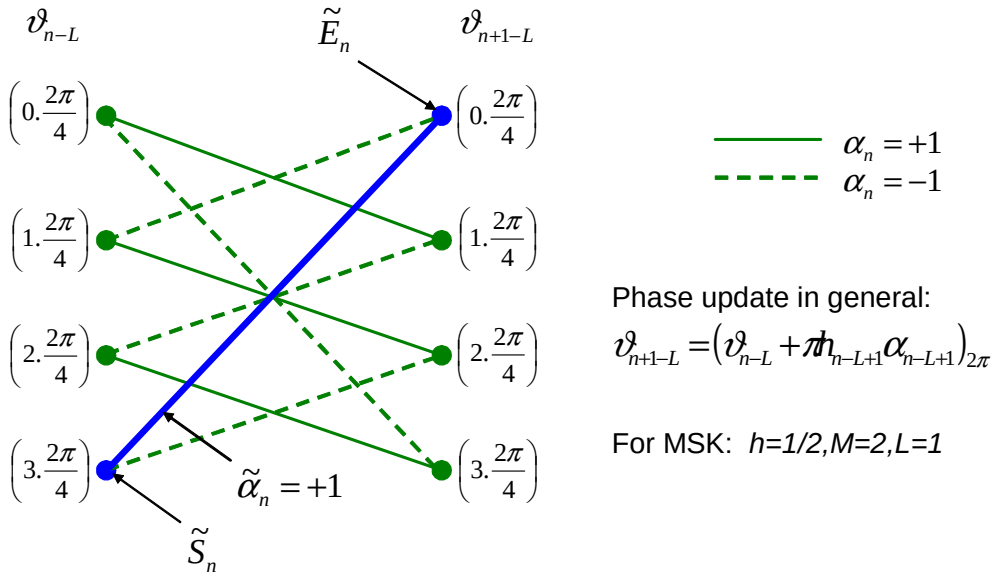

Figure 2.2. MSK Trellis.

where

$$z_n(\widetilde{\boldsymbol{\alpha}}_n) = \int_{nT_s}^{(n+1)T_s} r(t)\; e^{-j2\pi \sum_{i=n-L+1}^{n} h_{\underline{i}}\widetilde{\alpha}_i q(t-iT_s)}dt \tag{2.7}$$

represents the matched filtering operation. $\widetilde{S}_n$ is the starting state for the *hypothesized* trellis branch to which the cumulative phase $\widetilde{\vartheta}_{n-L}$ is associated and $\widetilde{E}_n$ is the ending state, $h_{\underline{i}}$ is the modulation index associated with $\widetilde{\alpha}_i$.[3]

The SISO processor for CPM incorporates the branch metrics from the matched filtering operation into the *max-log* version of the algorithm in [12], which does not require any knowledge of the noise psd N_0. The SISO processor may also use any available knowledge of the probability distribution of the *block* of information symbols $\widetilde{\boldsymbol{\alpha}}$ to do the decoding from the noise affected received waveform. When error control coding is used, the a prior knowledge of the probability distribution of $\widetilde{\boldsymbol{\alpha}}$ is obtained

[3] $(\widetilde{\vartheta}_{n-L}, \widetilde{\boldsymbol{\alpha}}_n)$ can be used to refer to the same branch $(\widetilde{S}_n, \widetilde{E}_n)$.

from the soft decision estimates of the channel symbols. In the absence of error control coding, *no assumption* is made on the same. The state metrics in the forward recursion are obtained by

$$A_n(\widetilde{E}_n) = \left[A_{n-1}(\widetilde{S}_{n-1}) + P_n\left[\widetilde{\alpha}_n; I\right] + \digamma_n(\widetilde{S}_n, \widetilde{E}_n)\right], \tag{2.8}$$

where $n = 1, 2, \ldots, K$. K is the length of the block over which the forward and reverse recursion state metrics are computed. Among the several branches ending at the state E_n, the *survivors* of the path metrics are used for cumulative metric update rather than a sum of the path metrics, which is the case in [12]. The path with the maximum (highest) cumulative metric is chosen as the survivor, the same way as in VA. No metric normalization is used. Also, $A_0(\cdot) = 0$ are *assumed* as initial conditions (*i.e.,* no assumption is made on the initial state of the CPM given by Eq. (1.8)). $P_n\left[\widetilde{\alpha}_n; I\right]$ represents the *a-priori* probability on the symbol α_n. Likewise, the state metrics in the reverse recursion are obtained by

$$B_n(\widetilde{S}_n) = \left[B_{n+1}(\widetilde{E}_{n+1}) + P_{n+1}\left[\widetilde{\alpha}_{n+1}; I\right] + \digamma_{n+1}(\widetilde{S}_{n+1}, \widetilde{E}_{n+1})\right], \tag{2.9}$$

where $n = K-1, \ldots, 1, 0$. Again, we assume $B_K(\cdot) = 0$. The soft decision of the information symbols[4] is obtained as

$$P_n\left[\hat{\alpha}_n; O\right] = \left[A_{n-1}(\widetilde{S}_{n-1}) + P_n\left[\widetilde{\alpha}_n; I\right] + \digamma_n(\widetilde{S}_n, \widetilde{E}_n) + B_{n+1}(\widetilde{E}_n)\right], \tag{2.10}$$

where $P_n\left[\hat{\alpha}_n; I\right]$ is the determined *a-posteriori* probability (APP) for the symbol α_n. The APP need to be adjusted in time (*aligned*) to spell out correct symbols in the case

[4]branch symbols of the trellis at time n

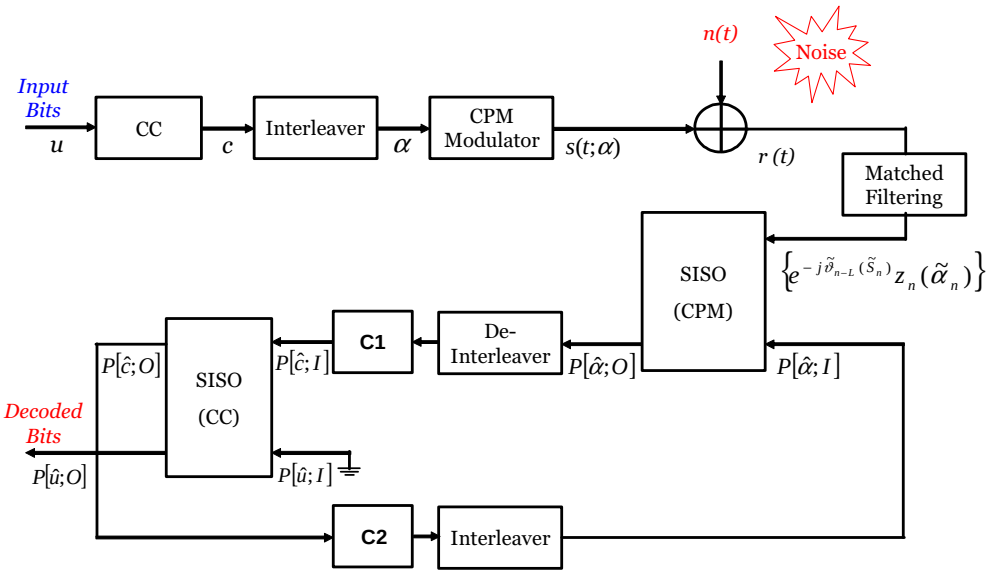

Figure 2.3. Serial Concatenation of CPM with CC.

of partial response CPMs. Finally, the APP are normalized with respect to the *a-priori* probability distribution given by

$$P_n(\hat{\boldsymbol{\alpha}}; O) = P_n(\hat{\boldsymbol{\alpha}}; O) - P_n(\tilde{\boldsymbol{\alpha}}; I). \tag{2.11}$$

2.3 Serial Concatenation of CPM

2.3.1 Background

Shannon's noisy channel coding theorem established the possibility of information transfer with arbitrarily low probability of error for rates of transmission less than the capacity of the channel. A lot of research work was carried out to design modulation and coding schemes which took the performance close to the Shannon's limit. While random codes meant exponentially large decoding complexity for even moderate sizes of data blocks, structured codes meant a trade off with distance properties of the code.

Turbo codes [13] were invented in an attempt to design *random like* codes by parallel concatenation of relatively simple constituent codes separated by an interleaver. In principle, the idea behind serial concatenation of modulation and error control coding is based upon the turbo decoding process.

The block diagram of a serially concatenated coded (SCC) system is shown in Fig. 2.3. It consists of an inner modulation and an outer code, separated by an interleaver. At the transmitter end, we have input bits, possibly from a source encoder. The bit stream is encoded by a CC. The encoded bits are mapped into symbols for CPMs with higher order signalling (quaternary, octal, etc) using *natural* or *gray* mapping. The system model assumes an AWGN channel. The SISO algorithm used is given in the Section 2.2. Since the CPM modulator operates on the coded (and interleaved) symbols of the input bits, the SISO processor for CPM uses the APP of the code symbols $P[\hat{c}; O]$ produced by the SISO decoder for CC. The SISO processor for CC operates on the de-interleaved APP of the CPM symbols $P[\hat{\alpha}; I]$ to produce the APP of the input bits to the system. Since the two decoders *exchange* decoded information with each other in an iterative process, there is a sharp improvement (see Fig. 2.5) in the performance of the system. Although the two SISO devices are each based on the ML decoding criterion, the overall decoding is *not* ML based since the burden of jointly decoding the inner and outer codes is decoupled [12, 13]. Thus the SCC systems are *reduced complexity* systems when compared to the ML decoding.

2.3.2 Error Events in CPM

In modulations with *memory* such as CPM, decoding algorithms produce dependent bit errors *although* the noise affecting the system is white (uncorrelated noise samples even at high sampling rates). An error event occurs when the decoding algorithm traces

a decoding path in the trellis, which differs from the actual path by a few symbols.[5] There can be several possible error events occurring with different probabilities in a CPM. For example in MSK, the *most* probable error event (shortest merging path) is when we have a sequence $\boldsymbol{\alpha}_1 = \{\ldots, -1, +1, \ldots\}$ at the transmitter and a decoded sequence $\boldsymbol{\alpha}_2 = \{\ldots, +1, -1, \ldots\}$ at the receiver which gives it an Euclidean distance of 2. This distance [5] can be computed by

$$d^2 = \frac{1}{2E_b} \int_{(R+L-1)T} |s(t; \boldsymbol{\alpha}_1) - s(t; \boldsymbol{\alpha}_2)|^2 \; dt, \tag{2.12}$$

where the *difference* between $\boldsymbol{\alpha}_1$ and $\boldsymbol{\alpha}_2$ is *nonzero* for a span of R symbols. The bit error rate (BER) for MSK is given by the union bound[6]

$$P_e \approx 2 \cdot Q\left(\sqrt{\frac{2E_b}{N_0}}\right). \tag{2.13}$$

2.3.3 Interleavers, Inner and Outer Codes

In general, the union bound for the BER in a CPM can consist of probabilities due to multiple error events which have different *distances* and can be expressed as

$$P_e = k_1 \cdot Q\left(\sqrt{\frac{d_1 E_b}{N_0}}\right) + k_2 \cdot Q\left(\sqrt{\frac{d_2 E_b}{N_0}}\right) + \ldots + k_l \cdot Q\left(\sqrt{\frac{d_l E_b}{N_0}}\right). \tag{2.14}$$

Interleavers *reduce* the coefficients $\{k_i\}_{i=0}^{l}$ associated with the error events and improve the system performance. In order that the interleaver should work, the inner code has to be *recursive* such as CPM while the outer codes have to be *non-recursive*. CCs are popularly used as outer codes. A CC is described by the code rate, the generator

[5] An error event in linear codes such as convolutional codes is defined as that path which merged back to the all-zero code path. The number of ones in the codeword gives the distance associated with the event.

[6] $Q(\cdot)$ is defined in Appendix A.

polynomials and the constraint length, which together describe the error control properties, bandwidth expansion and the coding gain. The choice of CPM parameters for the inner code (h, M), the mapping rule (*natural/gray*) and the rate of the outer code (R_{cc}) are discussed in sufficient detail in [8]. All the SCC systems studied have been chosen to be *compliant* with these guidelines. The coefficient out *in front of* the $Q(\cdot)$ function also depends on the rule used to map bits to symbols and consequently may result in different bit error rates. For example, in the case of the multi-h CPM given by $h = \{\frac{4}{16}, \frac{5}{16}\}$, $M = 4$, 3RC, the performance of *gray* mapping is marginally better than *natural* mapping as seen in Fig. 2.4.

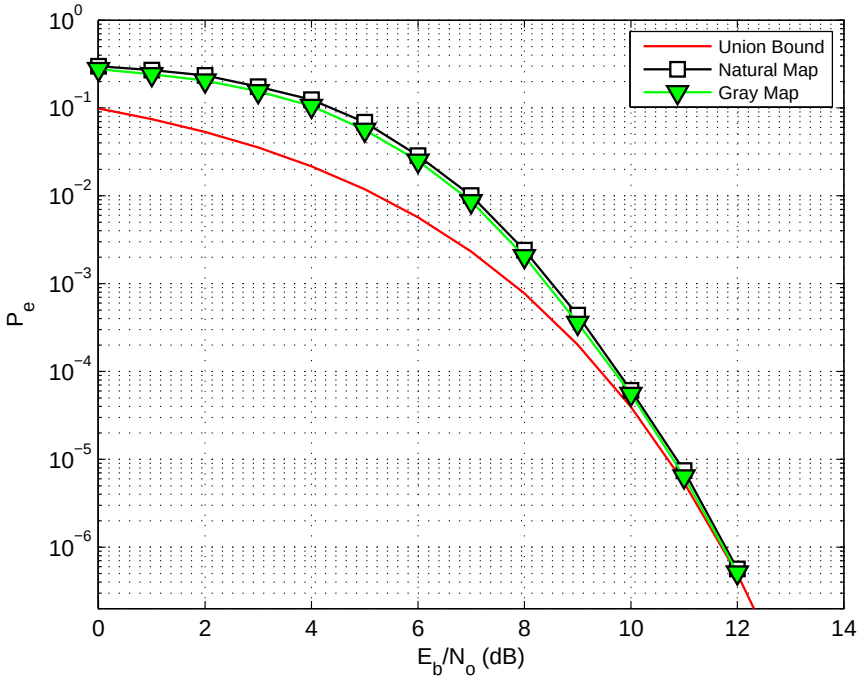

Figure 2.4. Natural vs. Gray Mapping.
CPM: $h = \{\frac{4}{16}, \frac{5}{16}\}$, $M = 4$, 3RC.

The interleavers used in SCC systems are *S-random* (pseudo random) interleavers. Block interleavers used to mitigate fast fading, will not be effective in SCC systems.

However, the S-random interleavers make the SCC CPM a little immune to fading, which is mentioned in [14]. Further, the coding gain of the SCC system greatly improves with the size of the interleaver. The complexity of the ML decoding exponentially increases with the size of the interleaver, just as they do with increased number of iterations. However, the decoding complexity is independent of the size of interleavers in SCC systems. But large interleavers increase latency in the decoding.[7] Performance of the SCC CPM system for varying number of iterations and interleaver sizes is shown in Fig. 2.5 and Fig. 2.6 respectively. The outer code under consideration is an optimal 4-state, rate $\frac{1}{2}$ convolutional code with the generator polynomials $g_1 = [1\ 0\ 1]$ and $g_2 = [1\ 1\ 1]$.

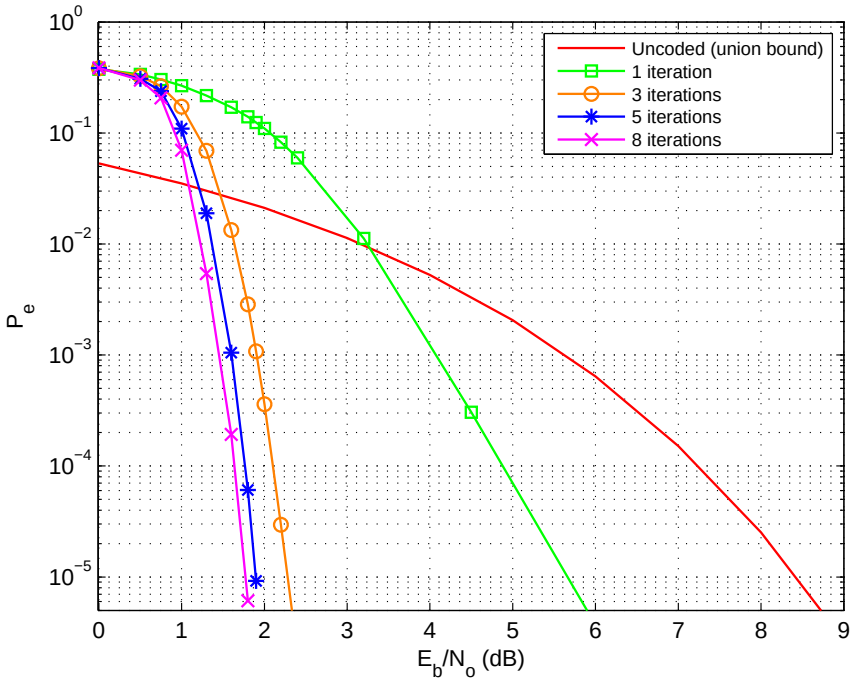

Figure 2.5. Coded PCM/FM: BER vs. # Iterations (2048 bit Interleaver).

[7] They also increase the complexity in terms of memory requirement.

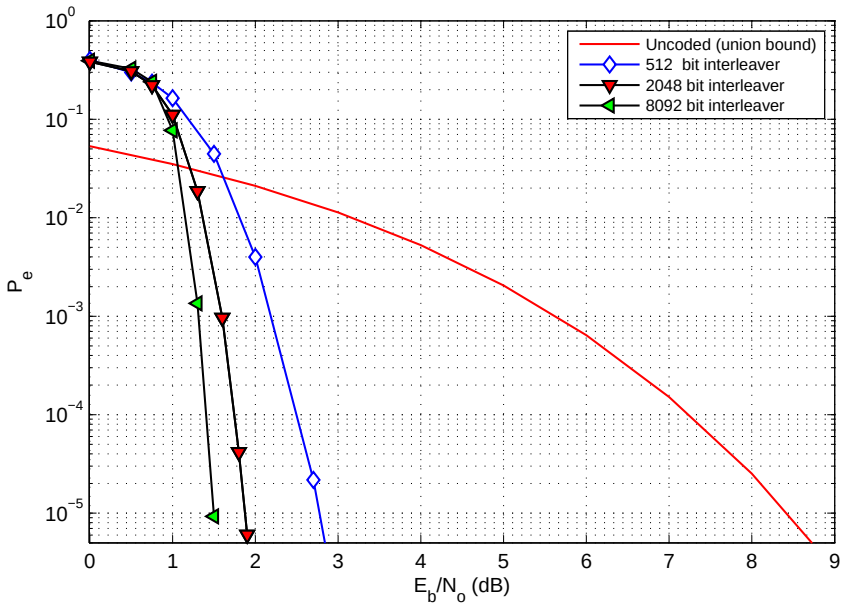

Figure 2.6. Coded PCM/FM: BER vs. Size of Interleaver (5 Iterations).

Chapter 3

Reduced Complexity Techniques for SCC-CPM

3.1 Introduction

It is well established in the literature and summarized in Chapter 2, that SCC systems with CPM as recursive inner codes give very high coding gains at low operative signal to noise ratios (SNR), and the performance approaches the union bound for the ML decoding. Although SCC systems by themselves are reduced complexity systems when compared to ML decoding, when very highly bandwidth efficient CPMs such as PCM/FM, SOQPSK-TG and ARTM [15] are used, they present a problem of extremely high decoding complexity at the receiver. Hence there is a *need* to develop complexity reduction techniques for SCC-CPMs..

Complexity reduction techniques attempt to reduce the size of the trellis as seen by the receiver. They use approximations to *sub-optimally* decode the CPM, in which case the signal models at the transmitter differs from the signal model at the receiver. This affects the Euclidean distances associated with the CPM error events. A way

to calculate the projected Euclidean distance is given in [16], which is also discussed in [17]. The ultimate aim of reduced complexity approaches is to achieve as good a performance as *optimal* decoding.[1] The amount of extra transmitter power needed to achieve performance close to optimal decoding serves as a *figure of merit* for each technique.

3.2 Rimoldi's Approach

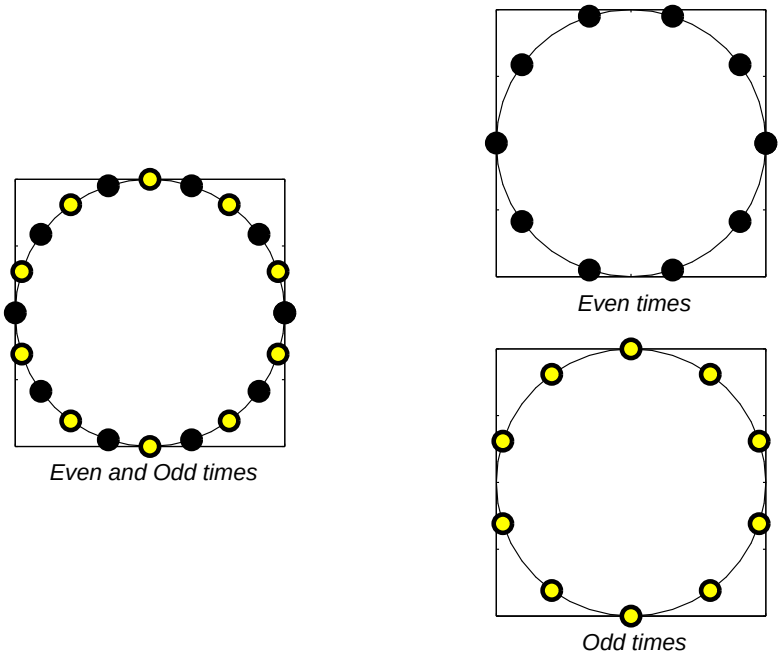

Figure 3.1. Complex Phase States at Even and Odd times in a CPM.

Using the *tilted phase* approach [18], Rimoldi identified that during any signalling interval, the CPM actually has only *half* the number of cumulative phases given by Eq. (1.10) *i.e.,* $P = P'/2$. This means that the optimal decoding itself requires PM^L states

[1] Here, it is important to note that optimal refers to the benchmark set by full complexity SCC CPM systems and not the ML decoding.

against $P'M^L$ states (see Eq. (1.8)). The phase state reduction is shown in Fig. 3.1. Hence we can write

$$h_{\underline{i}} = \frac{K_{\underline{i}}}{P}. \tag{3.1}$$

To realize Rimoldi's technique, we use the *pseudo* data symbols $u_i = \frac{(\alpha_i + M - 1)}{2}$ in the description of cumulative phase tilt ϑ_{n-L}. This transformation *decomposes* ϑ_{n-L} in Eq. (1.10) into a deterministic *data independent* phase tilt ν_{n-L} and a *data dependent* phase state θ_{n-L}, given by

$$\vartheta_{n-L} = \frac{2\pi}{P'} \sum_{i=0}^{n-L} K_{\underline{i}} \alpha_i = \frac{2\pi}{P} \sum_{i=0}^{n-L} K_{\underline{i}} u_i - \frac{(M-1)\pi}{P} \sum_{i=0}^{n-L} K_{\underline{i}}, \tag{3.2}$$

which can be written as

$$\vartheta_{n-L} = \theta_{n-L} + \nu_{n-L}, \tag{3.3}$$

where

$$\theta_{n-L} = \frac{2\pi}{P} \sum_{i=0}^{n-L} K_{\underline{i}} u_i, \tag{3.4}$$

and

$$\nu_{n-L} = -\frac{(M-1)\pi}{P} \sum_{i=0}^{n-L} K_{\underline{i}}. \tag{3.5}$$

The *data independent* phase tilt ν_{n-L} can be recursively obtained through

$$\nu_{n-L} = \nu_{n-L-1} - h_{\underline{n-L}}(M-1)\pi, \tag{3.6}$$

which gives the required phase correction in transition from the even phase states to the odd phase states and vice-versa. The term θ_{n-L} can take on P values resulting from the *modulo* 2π property of the complex phase, given by $\theta_{n-L} \in \{\frac{0\cdot 2\pi}{P}, \frac{1\cdot 2\pi}{P}, \frac{2\cdot 2\pi}{P}, \ldots, \frac{(P-1)\cdot 2\pi}{P}\}$ and similarly we have P' values of ν_{n-L} given by $\nu_{n-L} \in \{\frac{0\cdot 2\pi}{P'}, \frac{1\cdot 2\pi}{P'}, \frac{2\cdot 2\pi}{P'}, \ldots, \frac{(P'-1)\cdot 2\pi}{P'}\}$.

The number of states (and branches) in the trellis reduces by *half* compared to the classical treatment in [5]. So a new *set* of branch metrics for the SISO algorithm with only half the phase multiplications is used *in place of* $\Gamma_n(\widetilde{S}_n, \widetilde{E}_n)$ (see Eq. (2.6)). The reduced metric computation is given by

$$\gamma_n(\widetilde{S}_n, \widetilde{E}_n) = \mathrm{Re}\left\{ e^{-j\nu_{n-L}} e^{-j\,\widetilde{\theta}_{n-L}(\widetilde{S}_n)} z_n(\widetilde{\boldsymbol{\alpha}}_n) \right\}, \tag{3.7}$$

where ν_{n-L} is obtained at every symbol time using (3.6). However, the correlative state vector for the matched filtering remains the same as before in (2.7), which gives the same number of matched filtering operations. Rimoldi's technique is a way of *optimal* decoding of the CPM, without any approximations and assumptions. It is not applicable to SOQPSK, which is not a regular CPM and has a slightly different signal model.

All the analyses in the subsequent sections are presented as further simplifications over the Rimoldi's technique. In the reduced complexity techniques that follow, the signal model assumed at the receiver is different from the actual signal model at the transmitter. In such cases, they are *mismatched* and the decoding is *sub-optimal*. The performance degradation of the reduced complexity technique depends on the projected Euclidean distance [16, 17].

3.3 Decision Feedback

Decision feedback is a method of reducing the number of phase states via the state space partitioning approach [9, 17]. The SISO algorithm computes PM^L branch metrics while using the Rimoldi's technique of optimal decoding. Among them, not all the branch metrics are *competitive*. A complexity reduction is achieved by reducing number of phase state multiplications (P_r) in the branch metric computations, where

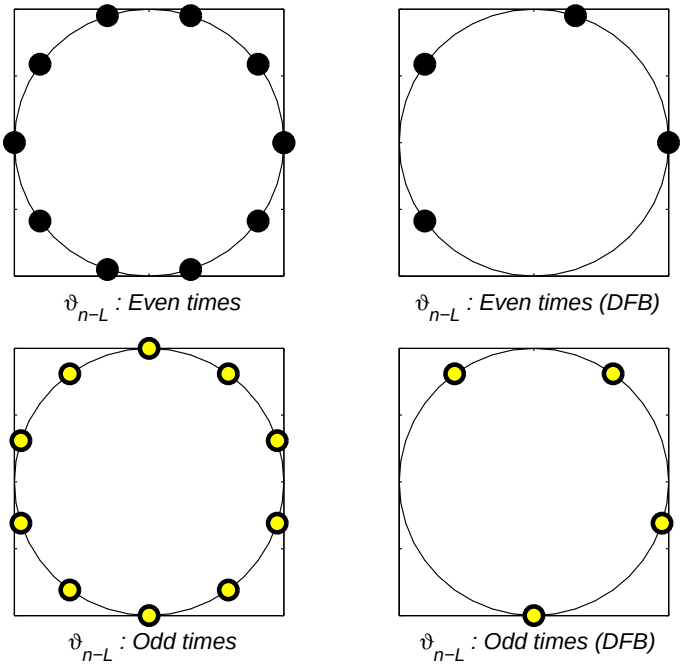

Figure 3.2. Complex Phase State Reduction by Decision Feedback.

$P_r < P$ as shown in Fig. 3.2. The phase state associations with the M^L matched filtered outputs are determined *at run time* by a phase update equation given by

$$\hat{\theta}_{n-L+1}(\widetilde{E}_n^f) = \hat{\theta}_{n-L}(\widetilde{S}_n^f) + \pi h_{\underline{n-L+1}} \hat{u}_{n-L+1}, \tag{3.8}$$

where $\widetilde{S}_n^f$ and $\widetilde{E}_n^f$ represent the states of the reduced trellis $\left(n(\widetilde{S}_n^f) < n(\widetilde{S}_n)\right)$ in the usual sense.[2] $\hat{u}_{n-L+1}$ represents the merging symbol (absorbed into the CPM state) for the state $\widetilde{S}_n^f$ and $h_{\underline{n-L+1}}$ is the *associated* modulation index. The metric computation for the SISO algorithm is given by

$$\urcorner_n(\widetilde{S}_n^f, \widetilde{E}_n^f) = \mathrm{Re}\left\{ e^{-j\nu_{n-L}} e^{-j\,\hat{\theta}_{n-L}(\widetilde{S}_n^f)} z_n(\widetilde{\boldsymbol{\alpha}}_n) \right\}. \tag{3.9}$$

[2] $n(\cdot)$ — number of values of $(\cdot)$

Both the phase tilt and cumulative phase updates in Eq. (3.6) and Eq. (3.8) are performed using the *merging* symbols from the *survivor* branches in the forward recursion which maximize the new state metric at time n (The time index in Eq. (3.6) refers to the update at time $n-1$ and not n). Decision feedback is a useful complexity reduction technique for CPMs with large number of phase states. Decision feedback applied to uncoded PCM/FM, ARTM CPM and SCC PCM/FM presented in Chapter 5, show a BER performance close to the full state optimal decoding, but at a much lesser complexity.

3.4 Pulse Truncation

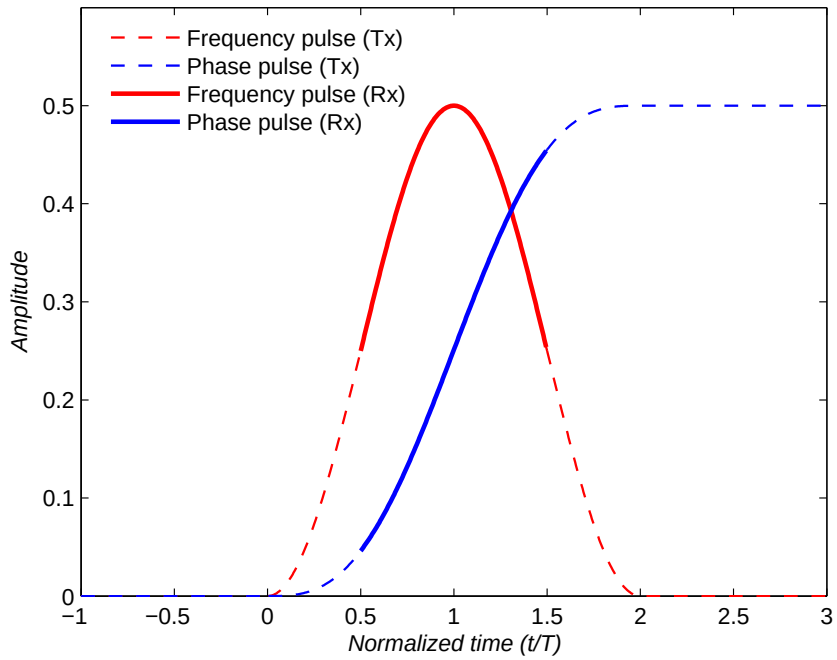

Figure 3.3. Pulse Truncation in PCM/FM.

The frequency pulse truncation is a useful complexity technique applicable to CPMs wit long and smooth phase pulses. Pulse truncation exploits the fact that the RC fre-

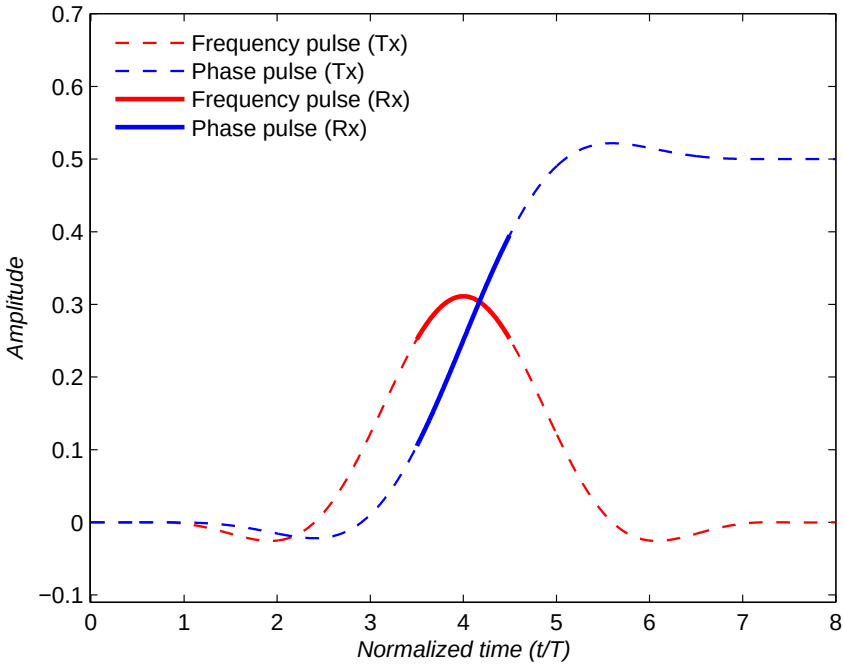

Figure 3.4. Pulse Truncation in SOQPSK-TG.

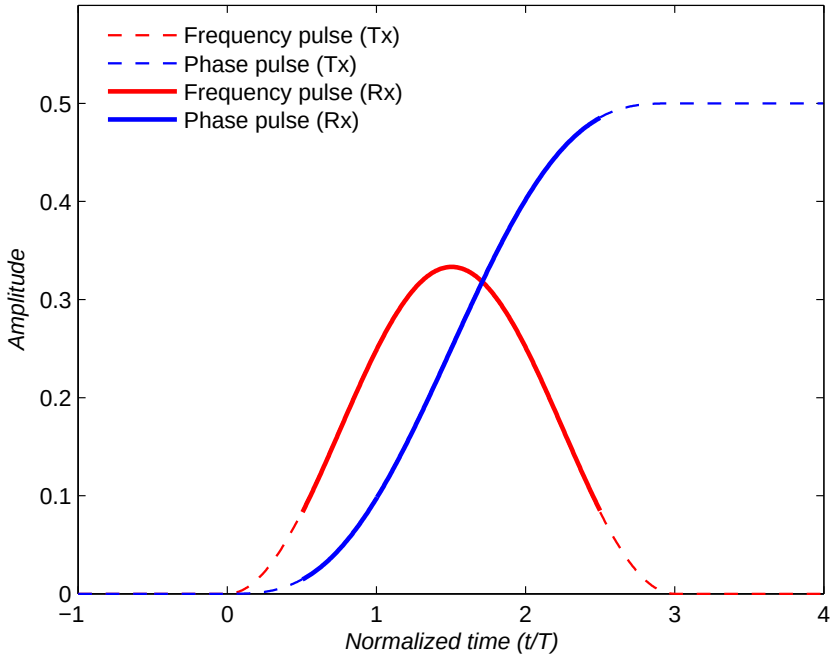

Figure 3.5. Pulse Truncation in ARTM.

quency pulse has a low frequency content on each end. This technique reduces the number of complex matched filtering operations due to correlative state reduction (and hence reduction in state complexity). For example in the CPMs:

- PCM/FM ($L = 2$): Truncation from $L = 2$ to $L_r = 1$ shown in Fig. 3.3 gives a complexity reduction by a factor of half. The reduced correlative state (see Eq. (1.7)) and the truncated pulse are given by

$$\boldsymbol{\alpha}_n^t = \alpha_n, \tag{3.10}$$

and

$$q_{PT}(t) = \begin{cases} 0, & t \leq \frac{T_s}{2} \\ q(t), & \frac{T_s}{2} \leq t \leq \frac{3T_s}{2} \\ \frac{1}{2}, & t \geq \frac{3T_s}{2} \end{cases} \quad \text{respectively.} \tag{3.11}$$

- SOQPSK-TG ($L = 8$): Truncation from $L = 8$ to $L_r = 1$ shown in Fig. 3.4 gives a complexity reduction by a factor of 128. The truncated pulse is given by

$$q_{PT}(t) = \begin{cases} 0, & t \leq \frac{7T_s}{2} \\ q(t), & \frac{7T_s}{2} \leq t \leq \frac{9T_s}{2} \\ \frac{1}{2}, & t \geq \frac{9T_s}{2}. \end{cases} \tag{3.12}$$

- ARTM ($L = 3$): Truncation from $L = 3$ to $L_r = 2$ shown in Fig. 3.5 gives a complexity reduction by a factor of 4. The reduced correlative state and the

truncated pulse are given by

$$\boldsymbol{\alpha}_n^t = \alpha_{n-1}, \alpha_n, \tag{3.13}$$

and

$$q_{PT}(t) = \begin{cases} 0, & t \leq \frac{T_s}{2} \\ q(t), & \frac{T_s}{2} \leq t \leq \frac{5T_s}{2} \\ \frac{1}{2}, & t \geq \frac{5T_s}{2} \end{cases} \quad \text{respectively.} \tag{3.14}$$

An enticing aspect in the decoding of SOQPSK (MIL and TG) lies in the fact that multiplication with any of the 4 phase states can otherwise be accomplished by change of signs associated with the real and complex parts of the matched filter output. So, the SOQPSK decoding is more easily implementable in hardware.

The metric computations for the SISO algorithm are given by

$$\gamma_n(\widetilde{S}_n^t, \widetilde{E}_n^t) = \text{Re}\left[e^{-j\nu_{n-L}} e^{-j\widetilde{\theta}_{n-L}(\widetilde{S}_n^t)} z_n(\widetilde{\boldsymbol{\alpha}}_n^t)\right], \tag{3.15}$$

where

$$z_n(\widetilde{\boldsymbol{\alpha}}_n^t) = \int_{nT_s}^{(n+1)T_s} r(t - DT_s)\; e^{-j2\pi \sum_{i=n-L_r+1}^{n} h_{\underline{i}} \widetilde{\alpha}_i q_{PT}(t - iT_s)} dt \tag{3.16}$$

gives the reduced number of matched filtering operations compared to Eq. 2.7. $\widetilde{S}_n^t$ and $\widetilde{E}_n^t$ represent the states in the reduced trellis. q_{PT} is the truncated pulse used at the receiver given by Eq. (3.11), Eq. (3.12) and Eq. (3.14) for the discussed cases of PCM/FM, SOQPSK-TG and ARTM, respectively. Likewise, the respective delays (in symbol times) needed to be incorporated into the received signal are given by $D = 0.5, 3.5, 0.5$ respectively.

3.5 Decision Feedback with Pulse Truncation

While decision feedback helps reduce the number of *phase states*, pulse truncation reduces the number of *phase states* and *complex matched filters*. A *combination* of the above two techniques gives *both* the advantages (although the loss depends on the overall approximation). The branch metrics for the SISO algorithm will now be

$$\lnot_n(\widetilde{S}_n^t, \widetilde{E}_n^t) = \text{Re}\left[e^{-j\nu_{n-L}} e^{-j\hat{\theta}_{n-L}(\widetilde{S}_n^{f,t})} z_n(\widetilde{\boldsymbol{\alpha}}_n^t)\right], \tag{3.17}$$

where $\widetilde{S}_n^{f,t}$ and $\widetilde{E}_n^{f,t}$ represent the states in the reduced trellis. Decision feedback, with pulse truncation gives huge savings in complexity in ARTM CPM, which is shown in Chapter 5. Another way of trellis reduction is achieved by the use of L_r at the receiver where $L_r > L$. Increase in the value of L however, allows further reduction in the number of phase states used compared to decision feedback. This technique as we see later, does not approximate to the optimal decoding at low SNR and consequently is suitable only for the uncoded systems. The metric increment for PCM/FM with $L_r = 3$ is given by

$$\lnot_n(\widetilde{S}_n^{f,\,L_r=3}, \widetilde{E}_n^{f,\,L_r=3}) = \text{Re}\left[e^{-j\nu_{n-3}} e^{-j\hat{\theta}_{n-3}(\widetilde{S}_n^{f,\,L_r=3})} e^{-j\pi h_{n-2}\hat{u}_{n-2}} z_n(\widetilde{\boldsymbol{\alpha}}_n)\right], \tag{3.18}$$

and the phase update equation is given by

$$\hat{\theta}_{n-3+1}(\widetilde{E}_n^{f,\,L_r=3}) = \hat{\theta}_{n-4+1}(\widetilde{S}_n^{f,\,L_r=3}) + \pi h_{n-2}\hat{u}_{n-2}, \tag{3.19}$$

where $\hat{u}_{n-2}$ is the merging symbol at time n. For $L_r = 4$, the metric increment is given by

$$\lnot_n(\widetilde{S}_n^{f,\,L_r=4}, \widetilde{E}_n^{f,\,L_r=4}) = \text{Re}\left[e^{-j\nu_{n-4}} e^{-j\hat{\theta}_{n-4}(\widetilde{S}_n^{f,\,L_r=4})} e^{-j\pi h_{n-3}\hat{u}_{n-3}} e^{-j\pi h_{n-2}\hat{u}_{n-2}} z_n(\widetilde{\boldsymbol{\alpha}}_n)\right], \tag{3.20}$$

and the phase update equation is given by

$$\hat{\theta}_{n-4+1}(\widetilde{E}_n^{f,\,L_r=3}) = \hat{\theta}_{n-5+1}(\widetilde{S}_n^{f,\,L_r=3}) + \pi h_{n-3}\hat{u}_{n-3}, \tag{3.21}$$

where $\hat{u}_{n-3}$ is the merging symbol at time n.

3.6 Implementation Issues

1. In decision feedback, P_r phase states take on values from the P phase states of the full state CPM. Since there are going to be finite and definite phase state values possible at any point of time, the phase update in Eq. (3.8) can be implemented in the *integer* domain as

$$\hat{I}_{n-L+1}(\widetilde{E}_n^f) = \left[\hat{I}_{n-L}(\widetilde{S}_n^f) + K_{\underline{n-L+1}}\hat{u}_{n-L+1}\right]_{\text{mod } P}, \tag{3.22}$$

where

$$\theta_{n-L} = \frac{\pi}{P}.I_{n-L} = \frac{\pi}{P}.\underbrace{\sum_{i=0}^{n-L} 2K_{\underline{i}}u_i}_{\textit{integer}}. \tag{3.23}$$

Thus, the complex phase updates and *modulo* 2π operations in Eq. (3.8) can be efficiently implemented using Eq. (3.22) and Eq. (3.23). The computed (updated) phase *indices* in Eq. (3.22) can be *mapped* back to the complex phase values using a *look-up* table of all the transmitter phase states, using the P_r values of indices

as the key as shown in Fig. 3.6. This idea can be extended to the computation of the data dependent phase terms in Eq. (3.18) – Eq. (3.21), as well as Eq. (3.5).

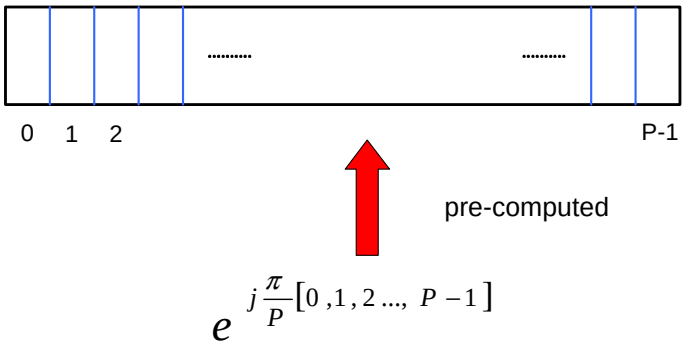

Figure 3.6. Lookup Table for Phase States.

2. In using the SISO algorithm, the initial values of the P_r phase states need to be suitably assumed. A guideline to choose the initial conditions of phase state indices is given by

$$I_{n-L} = \left[\underbrace{0,0,\ldots,0}_{M^{L_r-1}}, \underbrace{1,1,\ldots,1}_{M^{L_r-1}}, \ldots, \underbrace{P_r-1, P_r-1, \ldots, P_r-1}_{M^{L_r-1}} \right], \qquad (3.24)$$

where $\theta_{n-L} = \frac{\pi}{P} I_{n-L}$ and $I_{n-L} \in \{0,1,\ldots,P-1\}$.

3. The SISO algorithms do not make any assumption on the initial conditions of the CPM or on the termination bits for the CC. So all the recursion metrics assume initial conditions to be *zero* as mentioned before. The CPM modulator may assume any initial conditions of $L-1$ symbols of the correlative state vector in Eq. (1.7). In all the simulations, these symbols have been chosen to be '1', without any loss of generalization.

4. Correlative state reduction calls for suitable *assumption* on the initial condition of the data independent phase tilt ν_{n-L} when the Rimoldi's technique is applied. The initial conditions assumed are given by Table 3.1 for PCM/FM and Table 3.2 for ARTM CPM. In the pulse truncation technique, since the CPM phase is

Case	L_r	*Initial condition for* ν_{n-L}
1	1	$h(M-1)\pi$
2	2	0
3	3	$h(M-1)\pi$
4	4	0

Table 3.1. Initial Conditions for Phase Tilt ν_{n-L} in PCM/FM.

Case	L_r	*Initial condition for* ν_{n-L}
1	1	$h_2(M-1)\pi$
2	2	$h_1(M-1)\pi$
3	3	0

Table 3.2. Initial Conditions for Phase Tilt ν_{n-L} in ARTM CPM.

being observed only in the truncated pulse interval, appropriate *delay* before the matched filtering needs to be introduced. The set of modulation indices used must correspond to the symbols in the correlative state vector in multi-h CPMs.

5. With *large interleavers* and *sufficient* number of iterations, the performance of the coded system approaches the union bounds for ML decoding. Given an application, it is a trade-off problem involving —

   - amount of memory available,
   - latency and available processing power, and

- performance.

6. Sometimes the probability distributions $P[\hat{\alpha}; O]$ and $P[\hat{c}; O]$ are scaled by constants C_1 and C_2, for improved coding gain at no additional cost of resources. The scale factors are chosen on a *trial and error* basis $(|C_1|, |C_2| \leq 1)$. The following table lists the scale factors used for the $(5, 7)$ convolution code (see Fig. 2.3).

Modulation	C_1	C_2
PCM/FM	0.65	0.65
SOQPSK-TG	0.80	0.75
SOQPSK-MIL	0.75	0.75

Table 3.3. APP scale factors for $(5, 7)$ Coded CPMs.

7. Symbol interleavers could be used for non-binary CPMs. Symbol interleavers have been shown to give higher coding gains compared to their counterparts in bit interleavers but have higher error floors. In addition, they have lesser complexity in terms of recursion metric computations in the SISO algorithm [19].

8. Sampling issues in communication systems have been extensively documented in the literature. The chosen sampling rate should not only ensure *minimal aliasing*, but also preserve the *fidelity of waveform*. [3]

[3] Inadequately sampled waveforms can deteriorate the Euclidean distance (detection efficiency).

3.7 Noise Bandwidth Calibration

The white noise affecting the SCC system can be written as $n(t) = n_I(t) + j\ n_Q(t)$. The total variance σ_n^2 is given by

$$\sigma_n^2 = \frac{N_{samp}}{\log_2(M)\ R_{cc}\ \frac{E_b}{N_0}},$$

where

$$\frac{E_b}{N_0} : \text{Bit-energy to noise ratio (linear scale, not in dB)},$$

$$N_{samp} : \text{Sampling rate at the receiver (\# samples/symbol)},$$

$$M : \text{Cardinality of the source alphabet},$$

$$R_{cc} : \text{Rate of the convolutional code}.$$

Chapter 4

Non-Coherent Detection of CPM

4.1 Introduction

The received signal representation in Eq. (2.1) represents an ideal system, where the receiver has complete knowledge of the carrier phase. This requires the use of a *phase locked loop* (PLL) in the receiver to track the carrier. A receiver of this kind is called as a *coherent receiver* and the detection is called *coherent detection*. However, due to the very low operative SNR, the coherent detection in SCC CPMs suffers from false locks, phase slips, loss of locks due to Doppler shift (fading), carrier frequency jitter, etc. In such situations, *non-coherent* detection is an attractive strategy. Not only does it eliminate the need for PLLs, but it also provides a way to recover the information bits in the presence of *phase noise*.

4.2 Previous Efforts

Although several non-coherent detection algorithms are available in the literature and are suitable for various modulation schemes, only a handful of them are applicable

to systems using error control coding as highlighted in [20]. [21] presents a way to do non-coherent sequence estimation by *linearizing* the CPM using Laurent's decomposition. The drawback of this algorithm is that it does not address to the needs of SCC systems. The authors of [21] have presented algorithms applicable to iterative processing in [22] applicable to non-coherent, fading and ISI channels. Although they have been demonstrated to be very superior in the presence of strong phase noise, they are computationally complex due to rectangular window averaging in obtaining the phase estimates and are usually applicable to simple modulations. This algorithm is not practical in an environment where computational power is limited and judiciously used. [10] considers non-coherent detection of SCC MSK, which uses an exponential window for complexity reduction via recursive phase updation. Still, sufficient complexity reduction is not achieved in the way the branch metrics are computed. For example, they require computationally complex bessel functions to be computed for every trellis branch for both the forward and reverse recursions of the SISO algorithm. Also, the SISO algorithm presented here compute cumulative branch metrics, rather than cumulative state metrics (see Chapter 2). Due to practical limitations (latency and memory), the size of interleavers used has to be limited, which is undesirable. Another aspect in [10] is that the computation equations are considered are not in the log domain unlike the SISO algorithm in Chapter 2. Inspired by the ideas in [23], [4], a very simple *heuristic* non-coherent detection scheme is presented. The proposed algorithm gives a performance close to the coherent detection at moderate phase noise environments (for example - aeronautical telemetry applications), with minimal increase in complexity compared to the optimal non-coherent detection in [10].

4.3 The Proposed Non-Coherent Algorithm

The complex baseband signal at the receiver affected by phase noise is given by

$$r(t) = e^{j\psi(t)} s(t; \boldsymbol{\alpha}) + n(t), \tag{4.1}$$

where $\psi(t)$ is the phase noise affecting the received signal. Also, the receiver has no knowledge of the carrier phase in the absence of the PLL (non-coherent detection).

The non coherent branch metric is given by

$$\urcorner_n(\widetilde{S}_n, \widetilde{E}_n) = \text{Re}\left\{ Q_n^*(\widetilde{S}_n)\; e^{-j\nu_{n-L}} e^{-j\,\widetilde{\theta}_{n-L}(\widetilde{S}_n)} z_n(\widetilde{\boldsymbol{\alpha}}_n) \right\}, \tag{4.2}$$

where the complex phase reference $Q_n(\cdot)$ is computed using an exponential window averaging of the previous phase references and is given by

$$Q_n(\widetilde{E}_n) = \kappa Q_{n-1}(\widetilde{S}_n) + (1-\kappa)\left\{ e^{-j\nu_{n-L}} e^{-j\,\widetilde{\theta}_{n-L}(\widetilde{S}_n)} \right\}. \tag{4.3}$$

The *forgetting* factor κ defines the rate at which the older phase estimates needs to be *forgotten*. Obviously, under larger phase noise, the window needs to be smaller *i.e.,* κ needs to be smaller and vice-versa. Under no phase noise and $\kappa = 1$, the metrics in Eq. (4.3) and Eq. (4.2) reduce to coherent detection given by Eq. (3.7). When $\kappa < 1$, the algorithm begins to track the unknown carrier phase and it is eliminated out in the metric computations. The lower the value of κ, the faster is the *acquisition time* to track the unknown carrier phase, but higher is the required signal power to achieve the performance of coherent detection. The phase reference updates in Eq. (4.3) are computed after the *local survivors* are declared.

4.4 Phase Noise Simulation

The phase noise $\psi(t)$ is assumed to be slowly varying such that it can be assumed to be constant in the duration of any symbol interval. The phase noise at the matched filter sampling instants can be represented by the auto regressive (AR) model

$$\psi(k) = \psi(k-1) + \psi'(k), \tag{4.4}$$

where $\{\psi'(k)\}$ are independent and identically distributed Gaussian random variables with *zero* mean and variance σ^2.

Since the value of the forgetting factor chosen κ defines the span of the exponential window for averaging out the phase noise, the best value of κ must be determined for a given value of phase noise and for a given modulation scheme.

4.5 Demerits of the Algorithm

- The algorithm may not be applicable to fading channels since the algorithm tracks only the phase variations and does not use any amplitude reference symbols as in [10].

Chapter 5

Simulation Results

In this chapter, various results on simplified detection schemes for PCM/FM, SOQPSK-MIL, SOQPSK-TG and ARTM CPM are presented. Performance loss at a BER of 10^{-5} is used as the *figure of merit* to evaluate each of the complexity reduction and the non-coherent detection techniques.

5.1 Serially Concatenated Coded PCM/FM System

An SCC system is developed here for the *first* time for PCM/FM. Performance of the system with various interleaver sizes is presented in Fig. 5.2, which is based on 5 iterations. The scale factors C_1 and C_2 are assumed to be 0.65 each, which was earlier mentioned in Table 3.3. The performance of the SCC PCM/FM system greatly improves with the size of interleavers. Since the coded system is always processed in blocks, we cannot in general use large blocks of data for transmission which would result in high processing delay. An interleaver size of 2048 is *chosen* as a good trade-off between processing time and performance gain.

With an interleaver size of 2048, the system performance is evaluated for varying

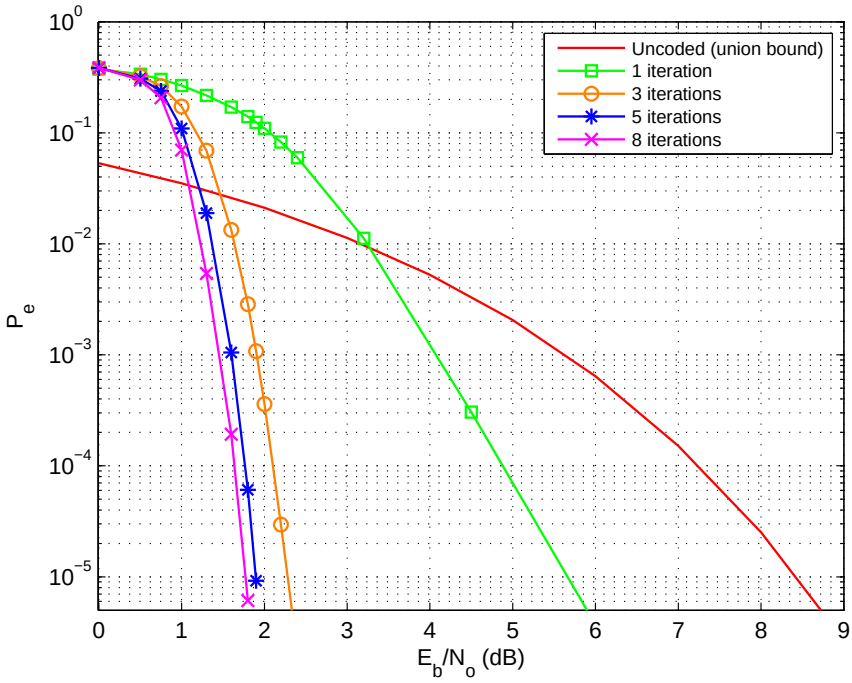

Figure 5.1. Coded PCM/FM: BER vs. # Iterations (2048 bit Interleaver).

number of iterations. Since the processing delay and complexity of the decoding algorithm depend on the number of iterations, we restrict number of iterations in the SCC system to some nominal value, which can give a nice trade-off between implementation complexity and performance gain. From the Fig. 5.1 we see that large coding gains are possible when the number of iterations are increased from 1 to 3. But, beyond 5 iterations, the BER performance of the system does not get significantly better. More than 5 iterations seem to only add to the decoding complexity. Hence, a maximum of 5 iterations seems to be a good choice. The choice of 2048 bit interleaver and 5 iterations is also guided by the fact that it gives us a fair chance to compare the performance of the SCC PCM/FM system to the performance of SCC SOQPSK-TG in [6], which is based on the same system parameters.

PCM/FM is a highly detection efficient CPM. A signal to noise ratio $\frac{E_b}{N_0}$ of around

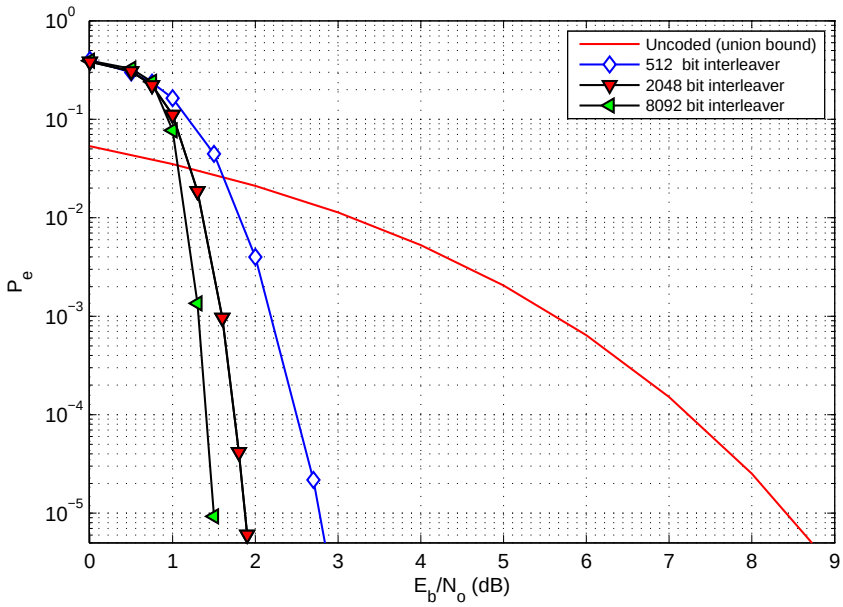

Figure 5.2. Coded PCM/FM: BER vs. Size of Interleaver (5 Iterations).

8.4 dB is needed to achieve a BER performance of 10^{-5}, without the use of error control coding. The same BER performance is achieved by the SCC PCM/FM system, with 6.55 dB savings in the transmitted signal power, which satisfies our requirement for a high gain system. However, the optimal decoding of PCM/FM requires a 20 trellis state representation and 4 complex matched filters. This is still computationally complex to be realized in digital hardware. So, several complexity reduction techniques have been applied for the *first* time to the SCC systems. The results are given in the next section.

5.2 Reduced Complexity Techniques for PCM/FM

The pulse truncation technique discussed in Section 3.4 is used, which reduces the number of complex matched filters to 2 and the number of trellis states to 10, resulting in a complexity reduction by half. The BER curve for the 10 state detector (denoted by $N_s = 10$ using $P_r = 10$, $L_r = 1$ closely approximates the optimal detection at all values

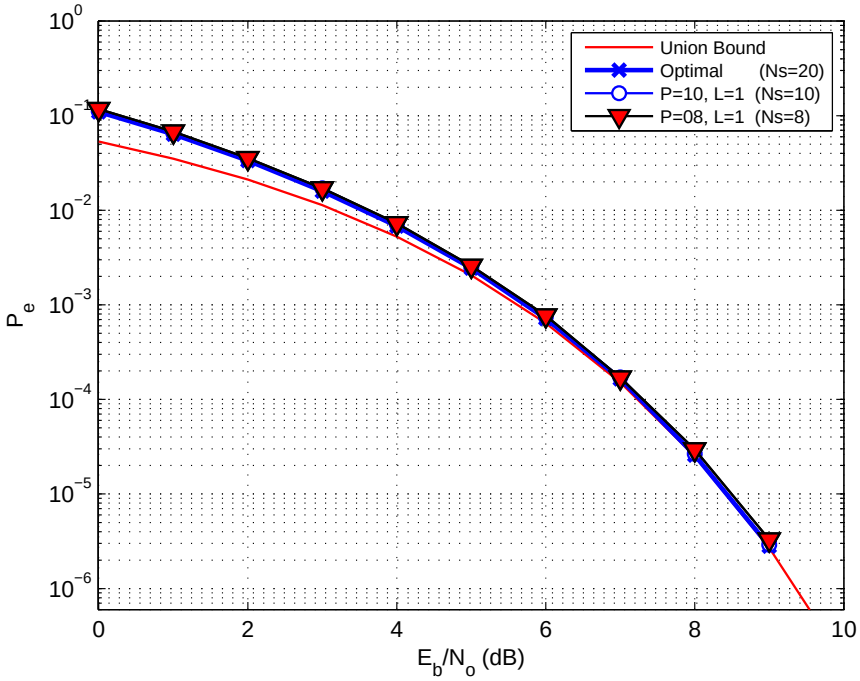

Figure 5.3. Reduced Complexity Techniques for Uncoded PCM/FM.

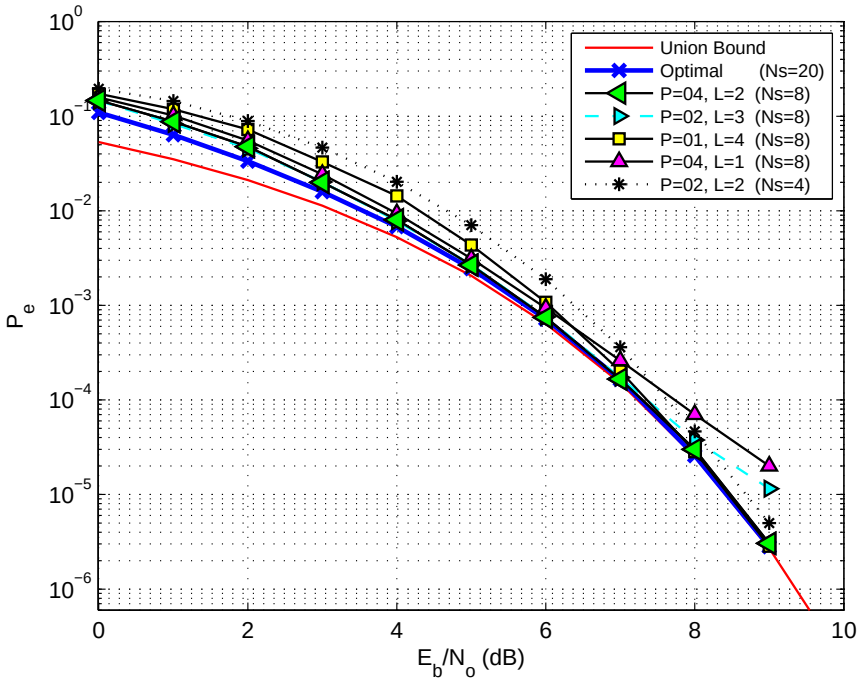

Figure 5.4. Other Reduced Complexity Techniques for Uncoded PCM/FM.

of $\frac{E_b}{N_0}$, and hence is a good technique to adopt to get a *near optimal* performance. The performance loss due to complexity reduction is measured in terms of the extra transmit power needed to achieve the optimal performance. The loss for the 10 state detector in the uncoded case is just 0.01 dB using pulse truncation. Further complexity reduction is possible by the use of decision feedback combined with pulse-truncation. An 8 state detector using $P_r = 8$, $L_r = 1$ is considered, which again gives a near optimal performance as shown in Fig. 5.3, with the loss in signal power due to approximation being 0.07 dB. Other cases of 8 state detectors given by $P_r = 4$, $L_r = 2$ and $P_r = 1$, $L_r = 4$ perform well at high $\frac{E_b}{N_o}$, but they do not approximate well, the optimal decoding curve at *low* $\frac{E_b}{N_o}$ as shown in Fig. 5.4. The performance of the *mismatched* detectors at low $\frac{E_b}{N_o}$

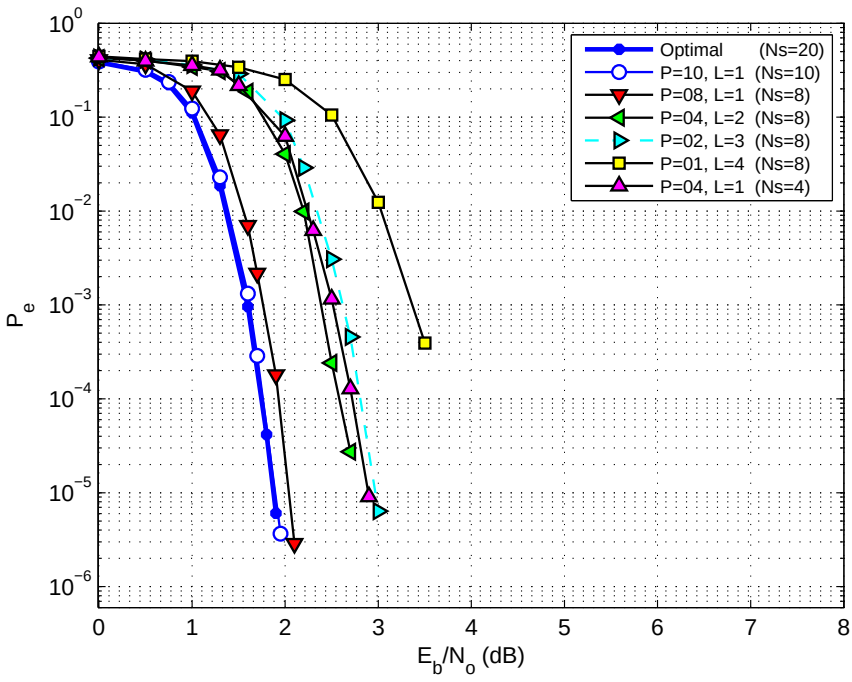

Figure 5.5. Reduced Complexity Techniques for Coded PCM/FM.

in the uncoded case is important because it indicates how well the curve approximates the optimal decoder in SCC system. As expected, the best approximations in the un-

coded case at low $\frac{E_b}{N_o}$, turn out to be the best approximations in the coded case as well. The 10 state detector described earlier, performs within 0.02 dB of the optimal detector for SCC PCM/FM as shown in Fig. 5.5. This means that the coding gain in the 10 state detector achieved over the optimal uncoded PCM/FM is 6.53 $(6.55 - 0.02)$ dB. This is the best result achieved in an attempt to look for low complexity high gain detectors. A simpler SCC PCM/FM detector with 8 states could be used with a performance loss of 0.17 dB. In any complexity reduction technique, the computational complexity trades off with performance loss. In general, a performance loss of the order of a tenth of a dB which is the case in the 10 state SCC PCM/FM detector is permissible. All the described performance metrics are summarized in Table 5.1.

Case	P_r	L_r	*Number of States*	*Number of MFs*	*Loss in dB Uncoded*	*Loss in dB Coded*	*Comments*
1	10	2	20	4	0	0	*Optimal*
2	10	1	10	2	0.01	0.02	*Recommended*
3	8	1	8	2	0.07	0.17	*Good*
4	4	1	4	2	> 1	1.01	*Not recommended*

Table 5.1. Comparison of Reduced Complexity Techniques for PCM/FM.

5.3 Reduced Complexity Techniques for ARTM CPM

ARTM CPM is a highly bandwidth efficient CPM. Optimal decoding of ARTM CPM requires a 256 state trellis representation and 64 complex matched filters. Optimal decoding is practically unaffordable in terms of the computational power required to get optimal performance. Pulse truncation technique is considered here, which reduces the number of complex matched filters to 16. The number of states in the reduced trellis is 64, which gives a complexity reduction by a factor of 4. The BER performance of the reduced complexity ARTM CPM detectors is presented in Fig. 5.6. The performance

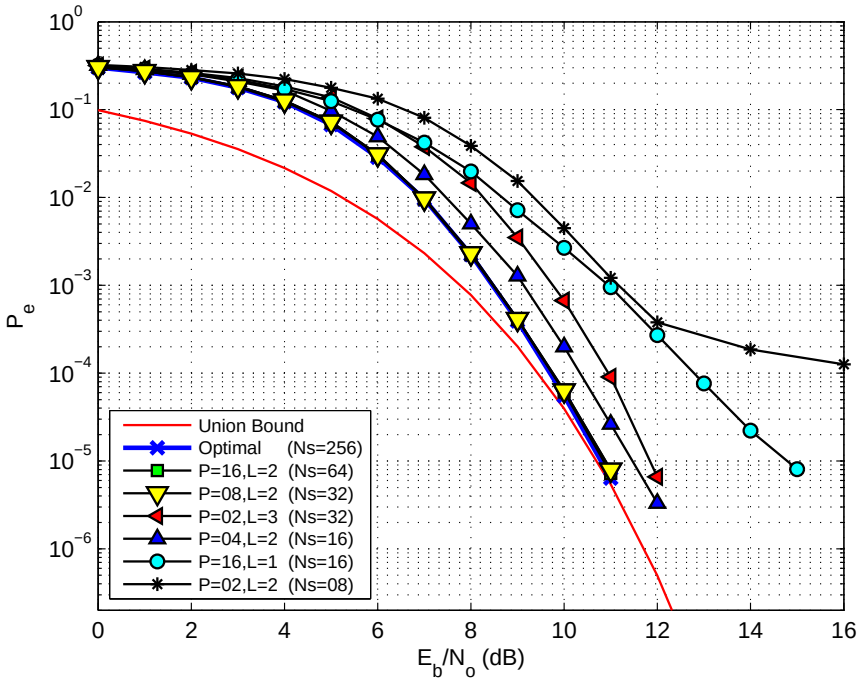

Figure 5.6. Reduced Complexity Techniques for Uncoded ARTM.

loss due to pulse truncation in the 64 state detector is 0.06 dB for uncoded ARTM CPM given by $P_r = 16$, $L_r = 2$. A further reduction in complexity is achieved when decision feedback with pulse truncation is considered using $P_r = 8$, $L_r = 2$. The performance loss for the 32 state detector is just 0.1 dB compared to the optimal 256 state detector. This means an 8 fold reduction in complexity is achieved for a near optimal decoding. The 32 state ARTM CPM detector approximates well to the optimal decoding at all values of $\frac{E_b}{N_o}$. A 16 state ARTM CPM detector for uncoded systems is also presented using the parameters $P_r = 4$, $L_r = 2$, which achieves a complexity reduction by a factor of 16 and suffers a performance loss of only 0.68 dB. The 32 state detector which gives near optimal in performance (loss of 0.1 dB) but with 8 times lesser complexity is recommended. Other reduced complexity detectors resulting by the use of parameters $P_r = 16$, $L_r = 1$ and $P_r = 2$, $L_r = 2$ give high performance loss of over 2 dB, in

comparison to the optimal decoding. The loss in performance is because the assumed signal model at the receiver is highly mismatched to the actual signal model which gives it poor distance properties (*i.e.,* bad approximations). A summary of some of the reduced complexity techniques for the uncoded ARTM CPM is given in Table 5.2.

Case	P_r	L_r	*Number of States*	*Number of MFs*	*Loss in dB Uncoded*	*Comments*
1	16	3	256	64	0	*Optimal*
2	16	2	64	16	0.06	*Near Optimal*
3	8	2	32	16	0.10	*Recommended*
4	4	2	16	16	0.68	*Good*

Table 5.2. Comparison of Reduced Complexity Techniques for ARTM CPM.

An SCC ARTM CPM could be developed on the lines of SCC PCM/FM and is suggested to be a possible future work.

5.4 Non-Coherent Detection of PCM/FM

The trellis based non-coherent detection algorithm presented in Chapter 4 is applied to PCM/FM. In the absence of phase noise, the standard deviation of phase noise is given by $\sigma = 0^{\circ}/\text{symbol}$. The non-coherent receiver does not assume any knowledge of the unknown carrier phase because of the absence of PLL. A forgetting factor κ is used to compute the complex phase reference metric by exponential window averaging in (4.3). The forgetting factor defines the rate at which the non-coherent algorithm tracks and acquires the unknown carrier phase. A smaller value of κ allows faster tracking of carrier phase, but affects the detection efficiency. The choice of κ decides the performance trade-off between detection efficiency and acquisition time. In practice, it is found that a forgetting factor of around $\kappa = 0.9$ is a good choice of parameter to

track the unknown carrier phase.

The performance of non-coherent detection of uncoded and coded PCM/FM is shown in Fig. 5.7. The coherent detection is the baseline for comparing the performance of the non-coherent detection. In the absence of phase noise, the uncoded non-coherent detector performs with a loss of 0.1 dB and the SCC non-coherent detector performs with a loss of 0.58 dB compared to the optimal state coherent detection.

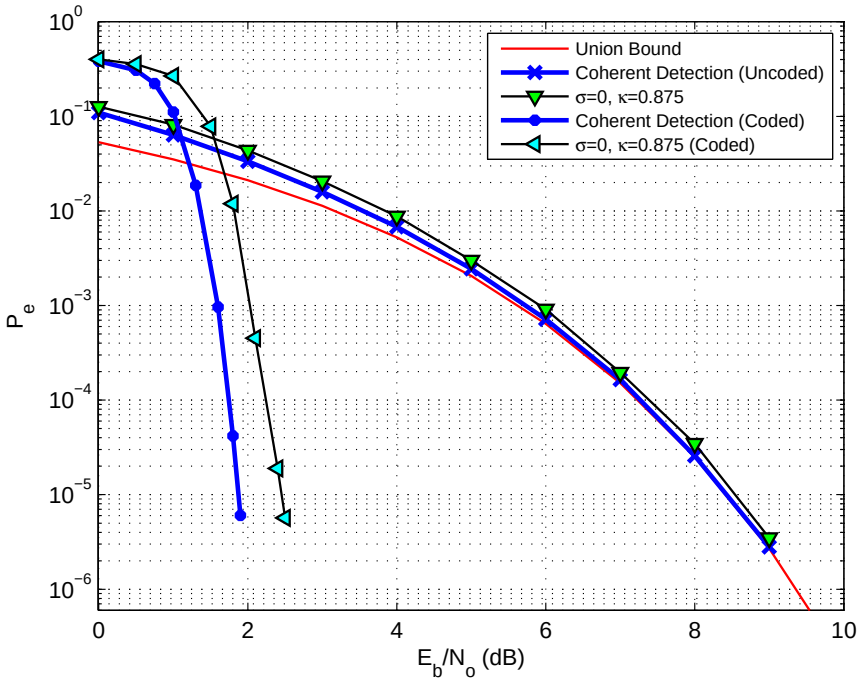

Figure 5.7. Non-Coherent PCM/FM: $\sigma = 0°$/sym.

In presence of a moderate phase noise, the performance of the non-coherent detector for different values of the forgetting factor κ. The best value of κ is chosen for a given variance (standard deviation) of phase noise. The performance of the non-coherent detector in moderate phase noise condition is given in Fig. 5.8 and Fig. 5.9. The best value of the forgetting factor κ is determined on a trial and error basis, in both the uncoded and coded systems. The SCC non-coherent detector performs within 0.35 dB

of the optimal coherent detector. This means that the lack of knowledge of the carrier phase and presence of moderate phase noise ($\sigma = 2^\circ/\text{symbol}$)[1] gives a performance as good as coherent detection but with an additional transmit power of just 0.35 dB.

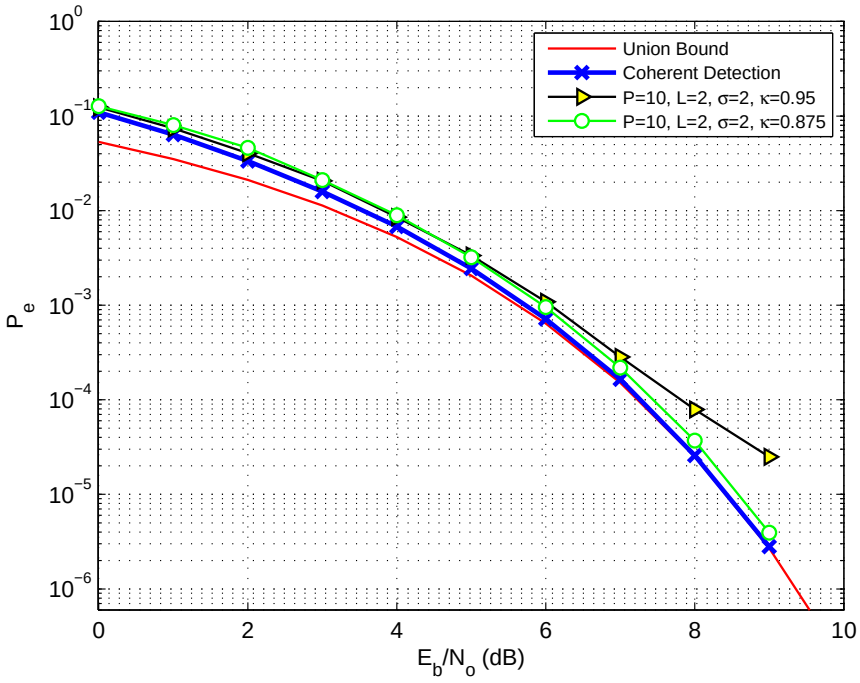

Figure 5.8. Non-Coherent PCM/FM (Uncoded): $\sigma = 2^\circ$/sym.

The performance of the non-coherent detector under higher phase noise conditions is shown in Fig. 5.10 and Fig. 5.11. The losses are much higher because of higher phase noise and also because of the fact that the decoding algorithm is heuristic and not optimal. The performance of the non-coherent detectors for select (best) cases of κ is summarized in Table 5.3.

The non-coherent detection is applied to the 10 state reduced complexity SCC PCM/FM. The performance of the reduced complexity non-coherent detector under moderate phase noise is shown in Fig. 5.12. The 10 state non-coherent detector is a

[1]From now on, phase noise is indicated in terms of the standard deviation σ.

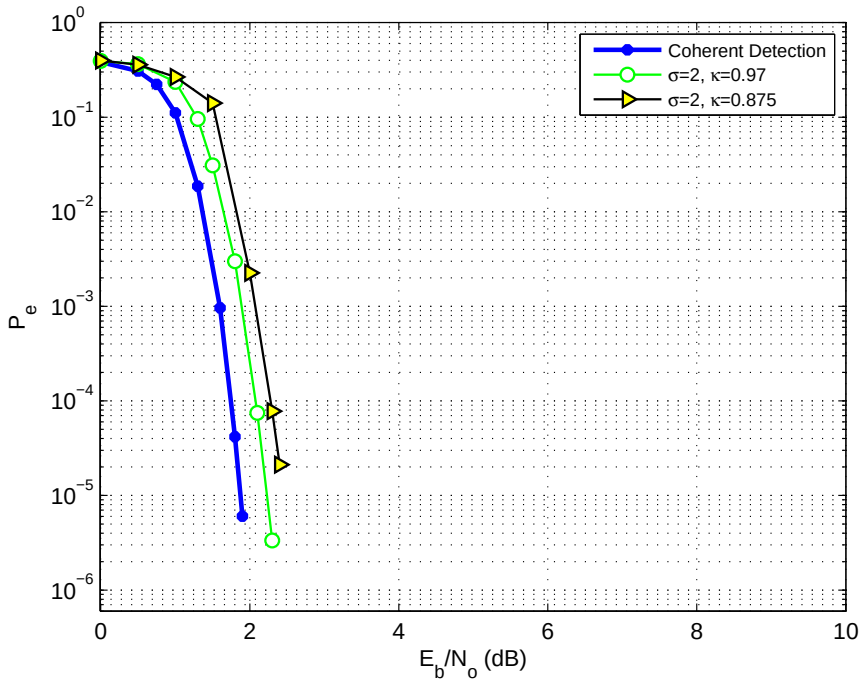

Figure 5.9. Non-Coherent PCM/FM (Coded): $\sigma = 2°$/sym.

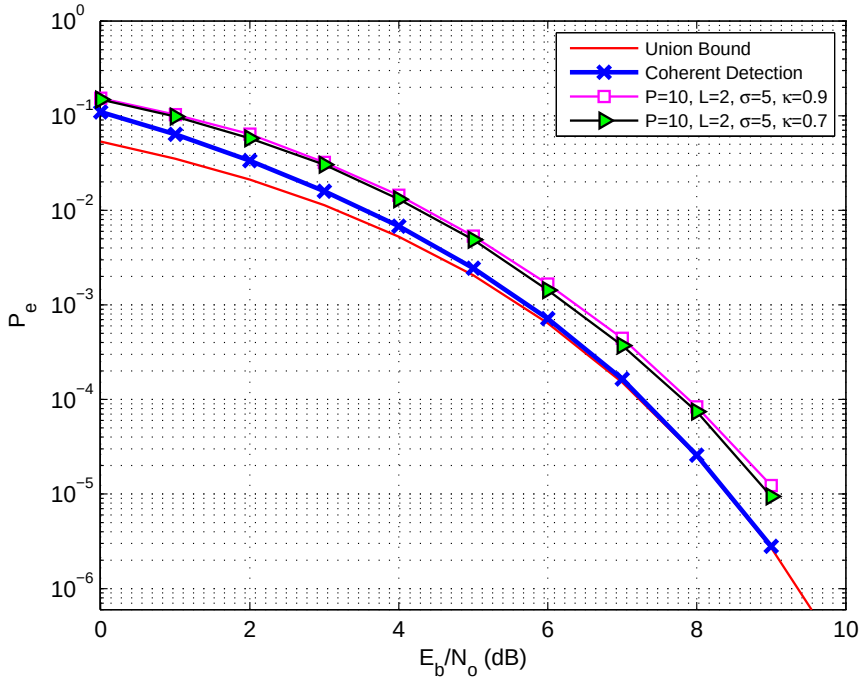

Figure 5.10. Non-Coherent PCM/FM (Uncoded): $\sigma = 5°$/sym.

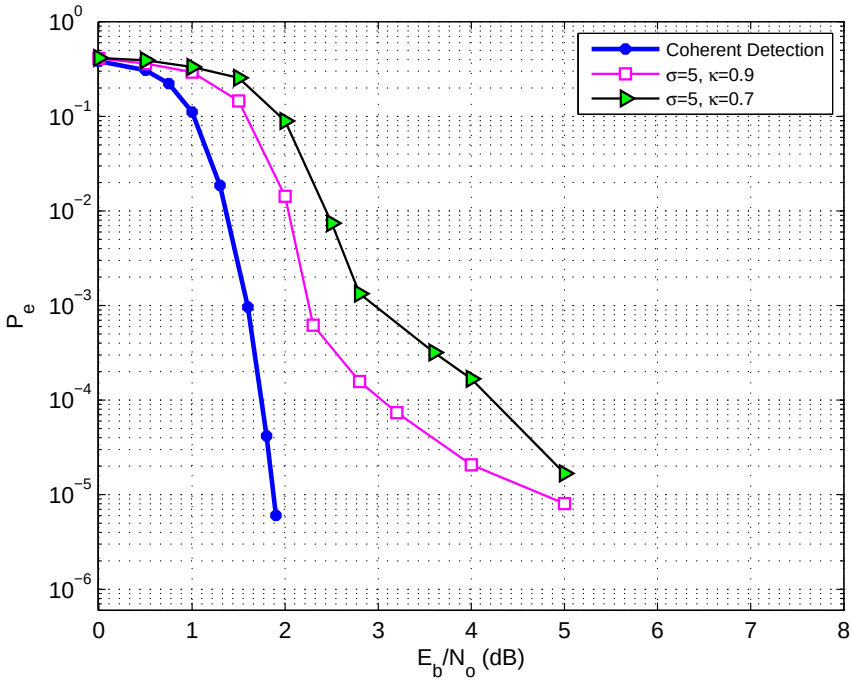

Figure 5.11. Non-Coherent PCM/FM (Coded): $\sigma = 5°$/sym.

reduced complexity high gain detector which performs within 0.4 dB of the optimal (20 state) coherent detector.

Case	*Phase Noise:* σ *(std.dev)*	*Loss in dB Uncoded*	*Loss in dB Coded*
1	$0°$	0.11	0.58
2	$2°$	0.15	0.33
3	$5°$	0.54	2.90

Table 5.3. Non-Coherent Detection of PCM/FM.

5.5 Non-Coherent Detection of SOQPSK-MIL

The performance of the 4 state non-coherent detector for SOQPSK-MIL is presented in Fig. 5.13 – Fig. 5.17. In the coded system, which is of interest to us, we

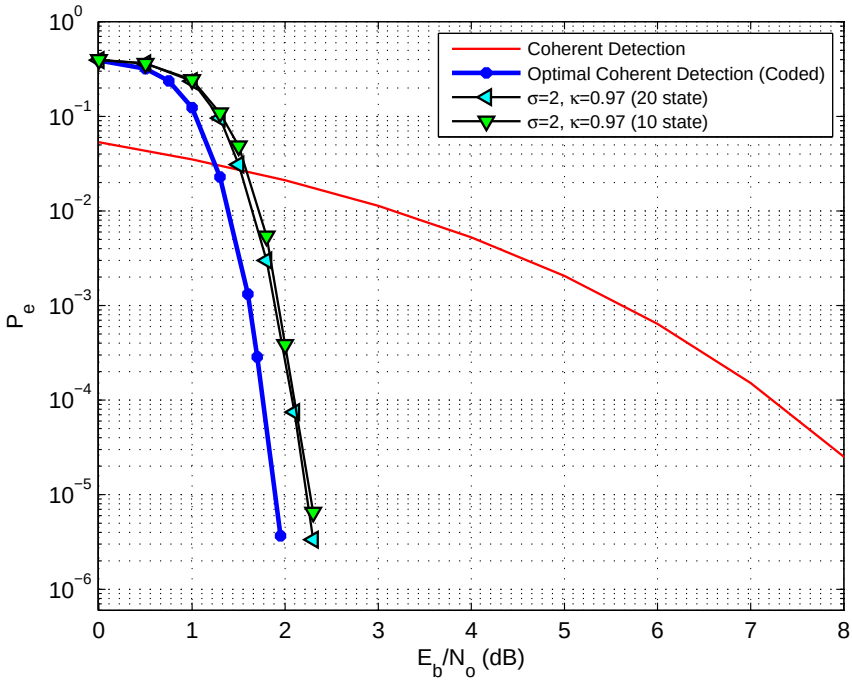

Figure 5.12. 10 state Non-Coherent PCM/FM (Coded): $\sigma = 2°$/sym.

see that the non-coherent detector makes a loss of 0.64 dB in the absence of phase noise, with the use of $\kappa = 0.875$. The Rimoldi's technique to do optimal decoding of SOQPSK with 2 states is not possible because SOQPSK is not a regular CPM and is defined by a slightly different CPM model which uses a precoder, discussed in Chapter 1.

The performance of the coded system under moderate phase noise conditions is given in Fig. 5.14 and Fig. 5.15. For a phase noise of $2°/$symbol, the best value of κ for the SCC non-coherent detector is 0.95 which performs with a loss 0.5 dB. As mentioned earlier, a slightly lower value of κ could be used allowing faster tracking of carrier phase without much compromise on performance (about 0.75 dB for $\kappa = 0.875$).

Under higher phase noise, the detector makes higher loss in performance as expected, shown in Fig. 5.16 and Fig. 5.17. It could be noted that the value of $\kappa = 0.875$

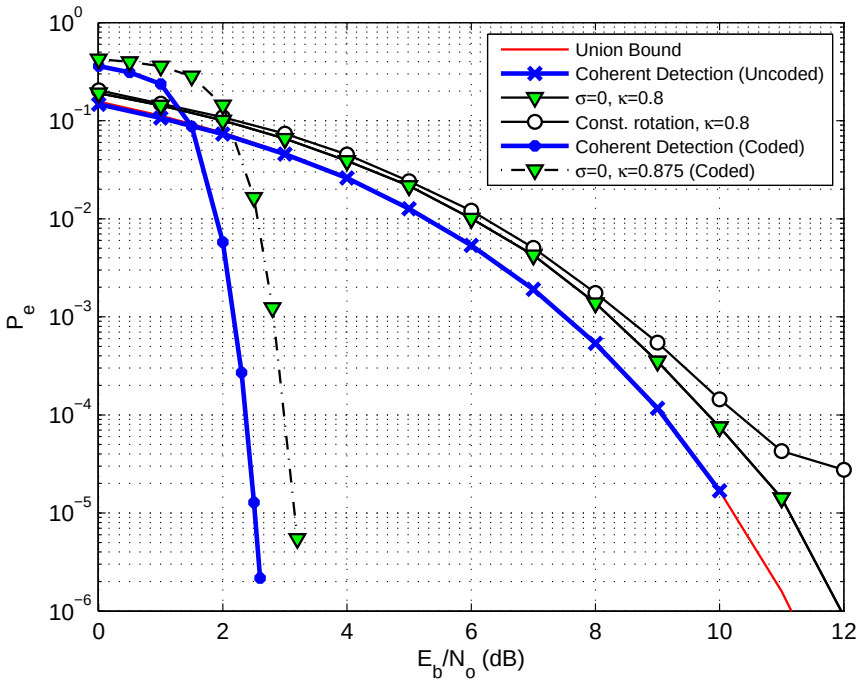

Figure 5.13. Non-Coherent SOQPSK-MIL: $\sigma = 0°$/sym.

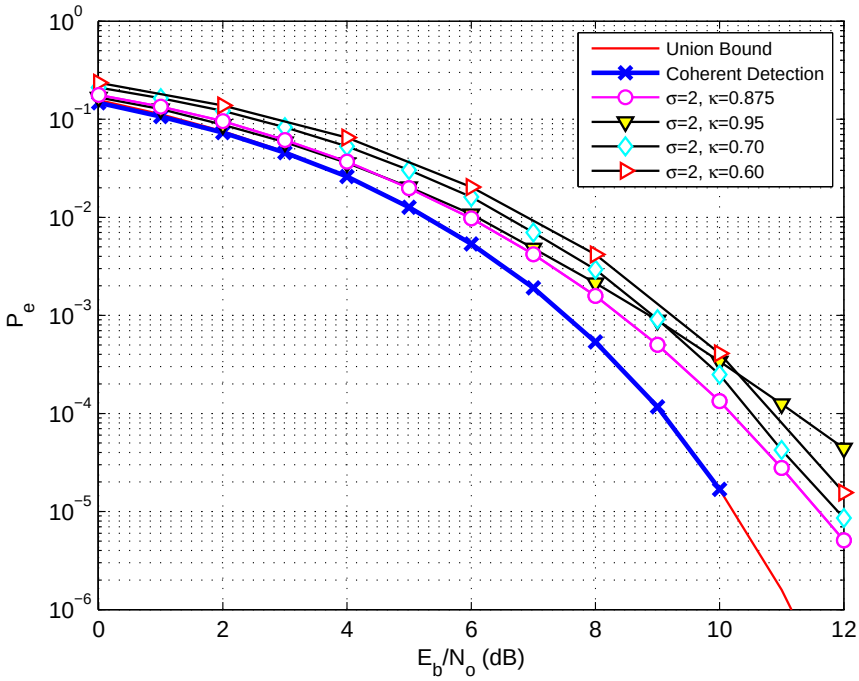

Figure 5.14. Non-Coherent SOQPSK-MIL (Uncoded): $\sigma = 2°$/sym.

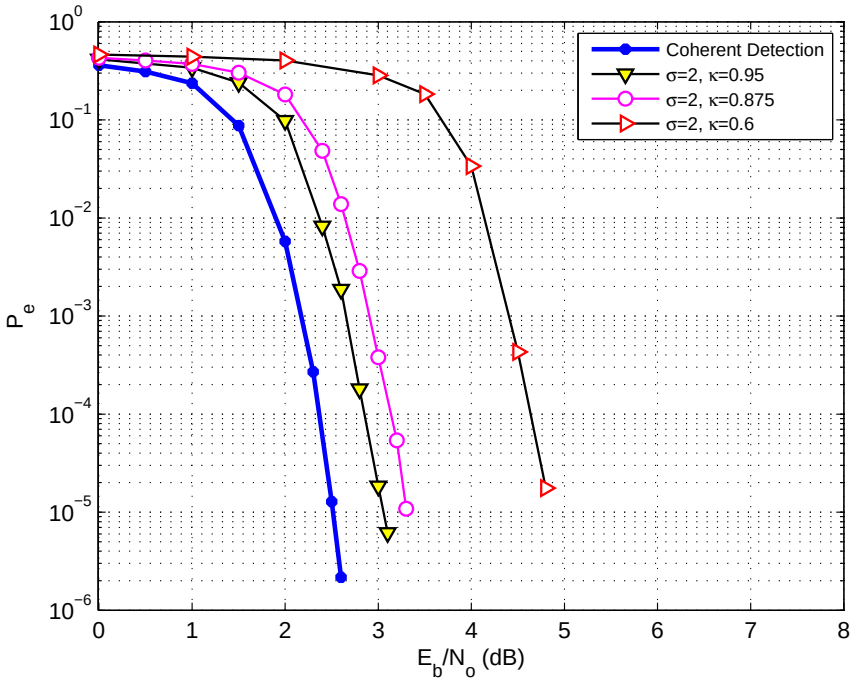

Figure 5.15. Non-Coherent SOQPSK-MIL (Coded): $\sigma = 2°$/sym.

is unsuitable for the uncoded system as shown in Fig. 5.16. But at low $\frac{E_b}{N_0}$, the BER curve with $\kappa = 0.875$ is better than the BER curve with $\kappa = 0.6$. This is the reason why $\kappa = 0.875$ performs better than $\kappa = 0.6$ in the coded system as shown in Fig. 5.17. The performance of the non-coherent detector for best cases of κ is summarized in Table 5.4.

Case	*Phase Noise:* σ *(std.dev)*	*Loss in dB Uncoded*	*Loss in dB Coded*
1	0°	0.90	0.64
2	2°	1.38	0.54
3	5°	3.95	1.40

Table 5.4. Non-Coherent Detection of SOQPSK-MIL.

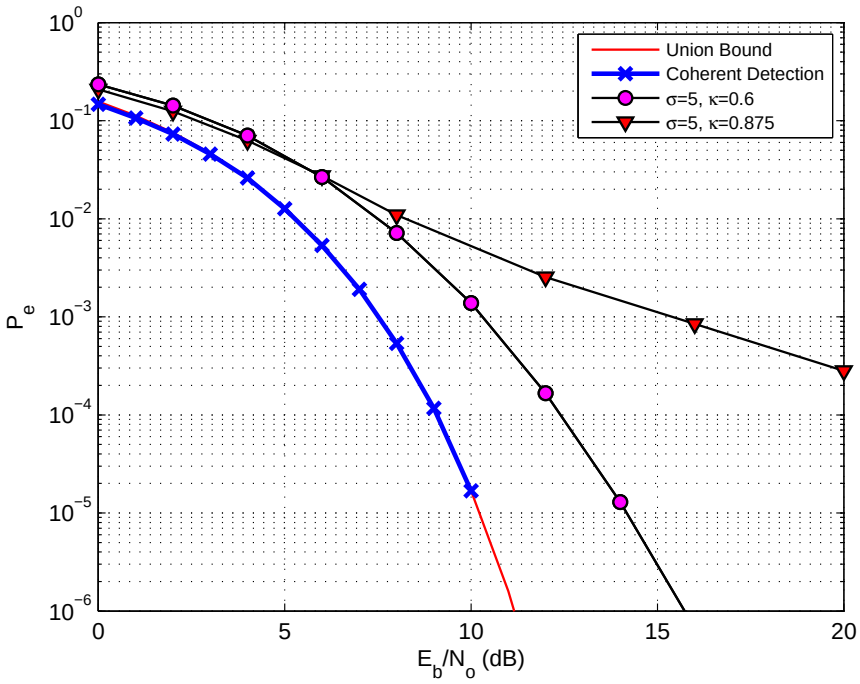

Figure 5.16. Non-Coherent SOQPSK-MIL (Uncoded): $\sigma = 5°$/sym.

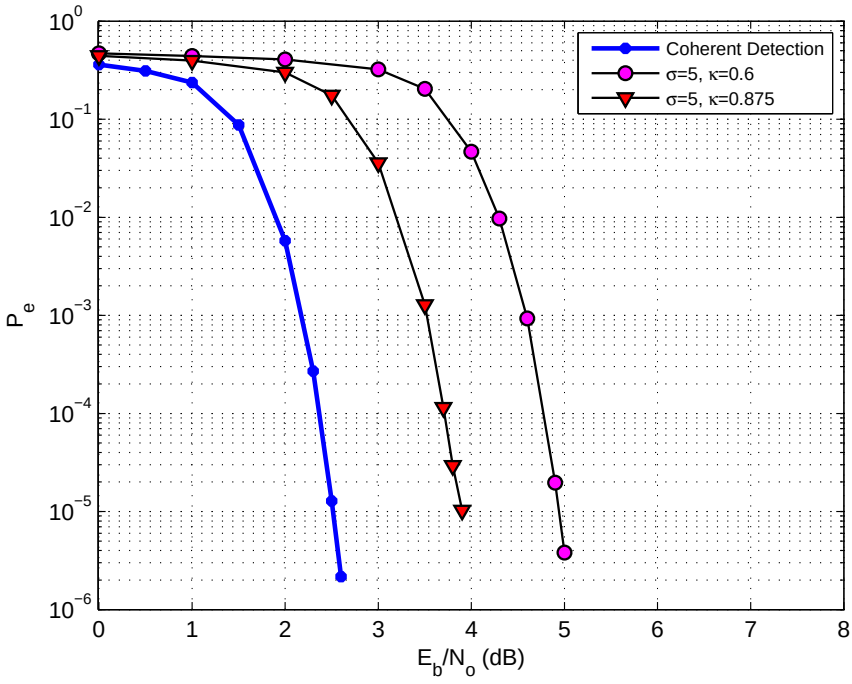

Figure 5.17. Non-Coherent SOQPSK-MIL (Coded): $\sigma = 5°$/sym.

5.6 Non-Coherent Detection of SOQPSK-TG

Optimal decoding of SOQPSK-TG requires a 512 state decoder which is not practical. Instead, the reduced complexity detector given in [6], shown to be near optimal is considered, which uses the pulse truncation to reduce the complexity by a factor of 128, but makes a performance loss of only about 0.2 dB compared to the optimal. The performance of the 4 state non-coherent detector for pulse truncated SOQPSK-TG is given in Fig. 5.18 – Fig. 5.22.

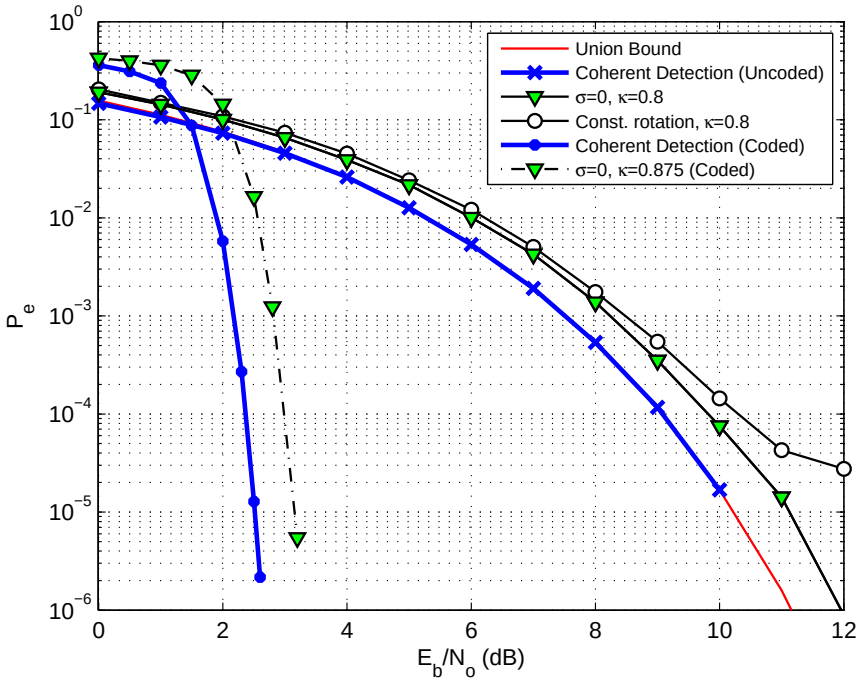

Figure 5.18. Non-Coherent SOQPSK-TG: $\sigma = 0°$/sym.

The performance of the non-coherent detector for SOQPSK-TG under no phase noise is given in Fig. 5.18. We see from Fig. 5.7, Fig. 5.13 and Fig. 5.18, that the performance loss gets higher for the non-coherent detector. The more bandwidth efficient SOQPSK-TG is harder to synchronize at the receiver than PCM/FM. The performance loss in SCC non-coherent detector is 0.79 dB under no phase noise conditions.

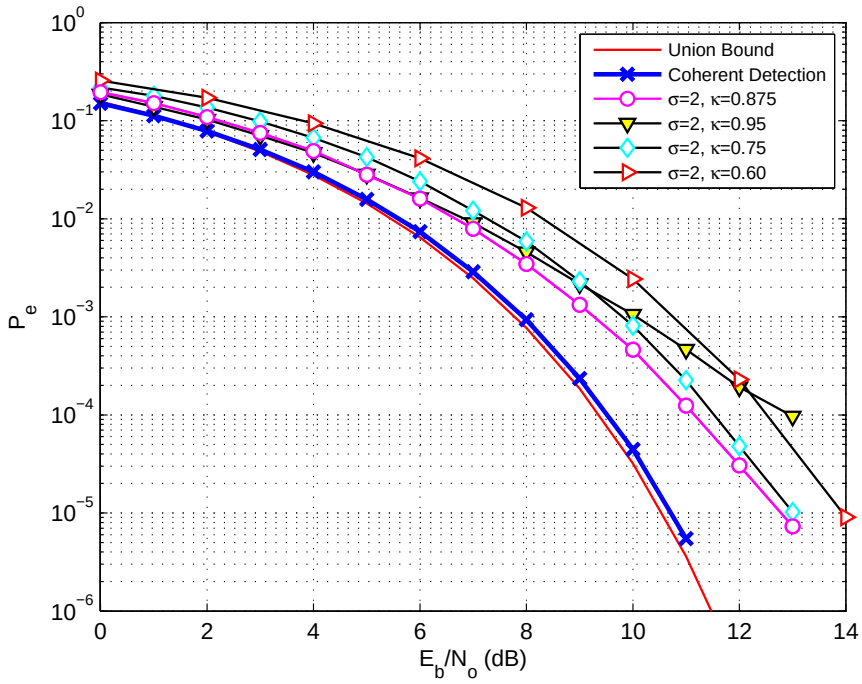

Figure 5.19. Non-Coherent SOQPSK-TG (Uncoded): $\sigma = 2°$/sym.

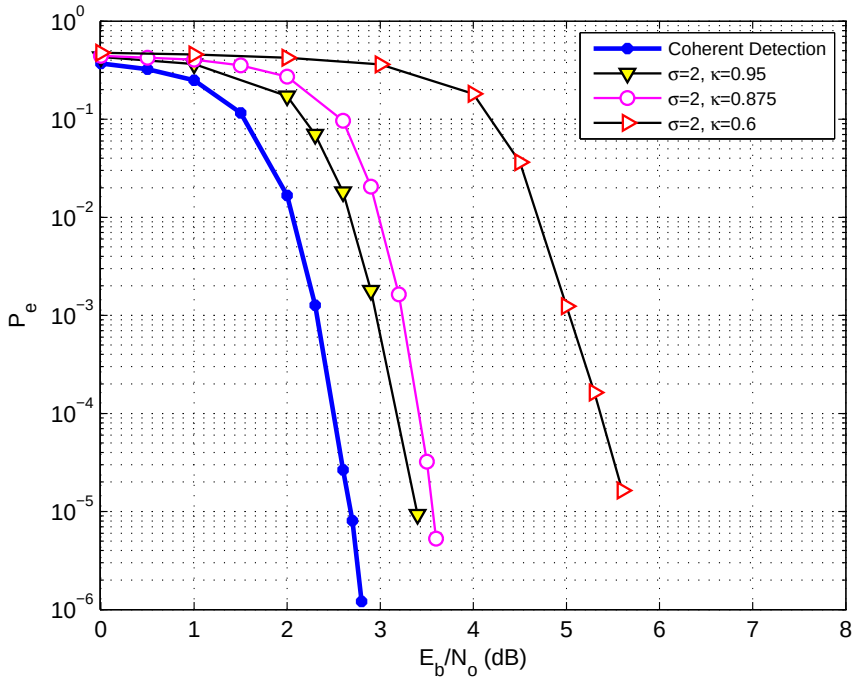

Figure 5.20. Non-Coherent SOQPSK-TG (Coded): $\sigma = 2°$/sym.

The performance of the non-coherent detector for moderate phase noise conditions is shown in Fig. 5.19 and Fig. 5.20 for uncoded and coded systems respectively.

Again as expected, the performance loss is higher with higher phase noise as shown in Fig. 5.21 and Fig. 5.22. As pointed out earlier in the case of SOQPSK-MIL, the best value of κ needed for a given phase noise, is to be determined separately for the uncoded and coded cases. The performance of the non-coherent detector for best cases of κ is summarized in Table 5.5.

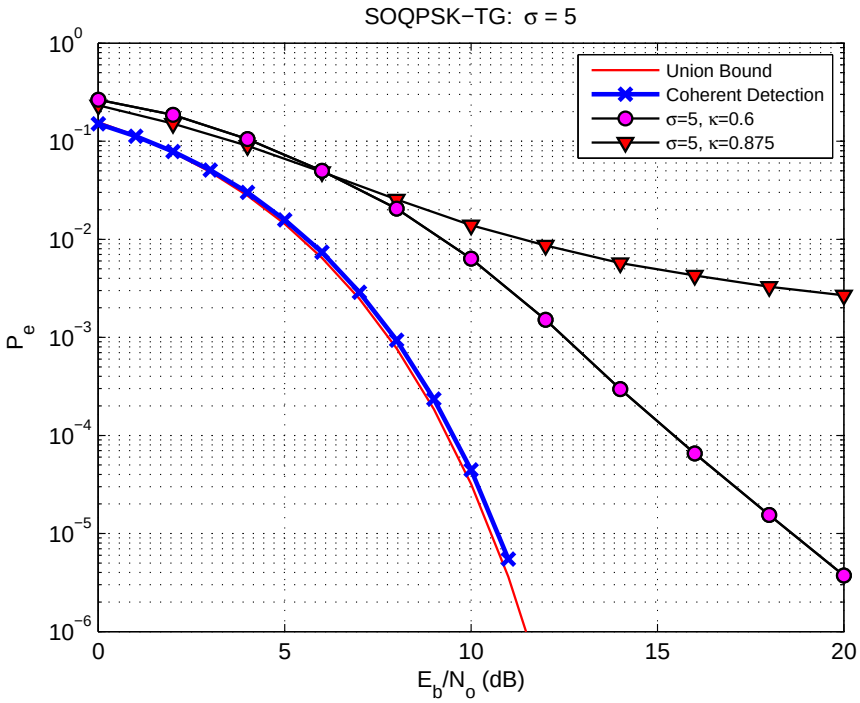

Figure 5.21. Non-Coherent SOQPSK-TG (Uncoded): $\sigma = 5°$/sym.

5.7 Non-Coherent Detection of ARTM CPM

ARTM CPM is the most bandwidth efficient of all the CPMs considered. A 256 state non-coherent detector for uncoded ARTM CPM is presented in Fig. 5.23. The

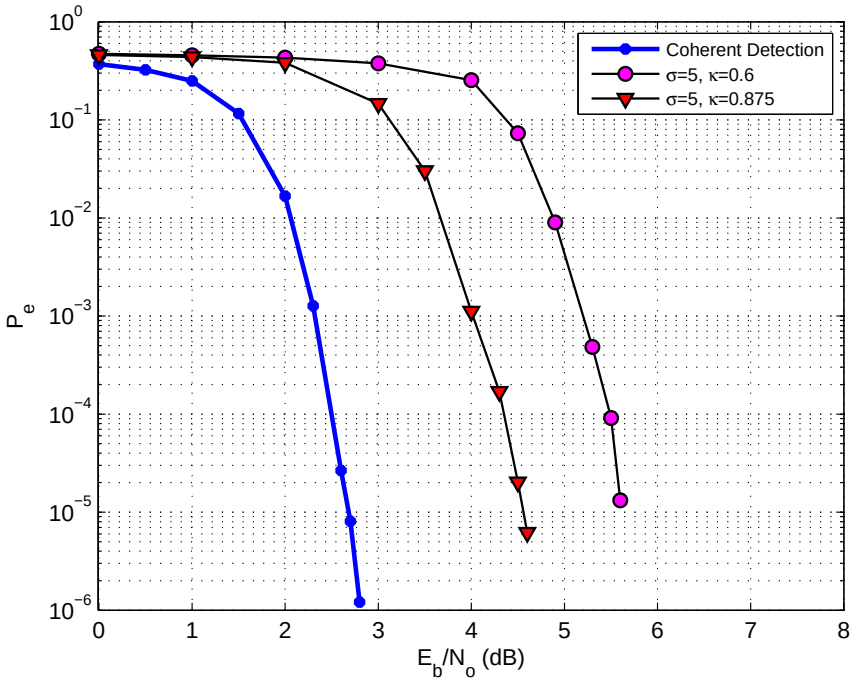

Figure 5.22. Non-Coherent SOQPSK-TG (Coded): $\sigma = 5°$/sym.

Case	*Phase Noise:* σ *(std.dev)*	*Loss in dB Uncoded*	*Loss in dB Coded*
1	0°	1.05	0.79
2	2°	2.07	0.71
3	5°	7.89	1.88

Table 5.5. Non-Coherent Detection of SOQPSK-TG.

non-coherent detector gives a performance loss of just 0.55 dB compared to the optimal coherent detection, under no phase noise conditions.

But, the 256 state detector is highly complex to be realized in digital hardware. So, the non-coherent detection is considered for the reduced complexity detectors presented in Section 5.3, shown in Fig. 5.24 and Fig. 5.25. The 16 state non-coherent ARTM CPM detector makes a performance loss of just 0.27 dB compared to the 16 state coherent detector, which itself is 0.68 dB worse than the optimal coherent detection. So, the 16

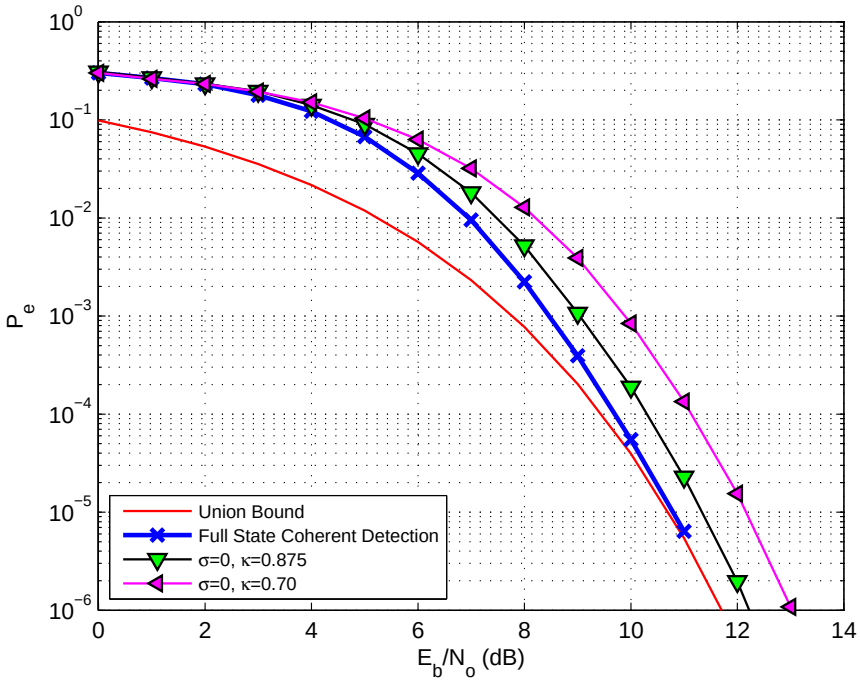

Figure 5.23. Non-Coherent ARTM CPM: $\sigma = 0°$/sym.

state non-coherent detector for ARTM CPM achieves a huge complexity reduction, by a factor of 16 compared to the optimal coherent receiver for ARTM CPM, but with a performance loss of less than 1 dB.

The performance of the non-coherent detector under moderate phase noise conditions given by $\sigma = 2°/\text{symbol}$ is shown in Fig. 5.26 – Fig. 5.28. The 16 state non-coherent detector shown in Fig. 5.28 gives a performance loss of just 0.37 dB compared to the 256 state non-coherent detector shown in Fig. 5.26. So a complexity reduction by a factor of 16 is achieved with the compromise in performance being only 0.37 dB. The performance of the non-coherent detector for full state ARTM CPM for the best cases of κ is summarized in Table 5.6.

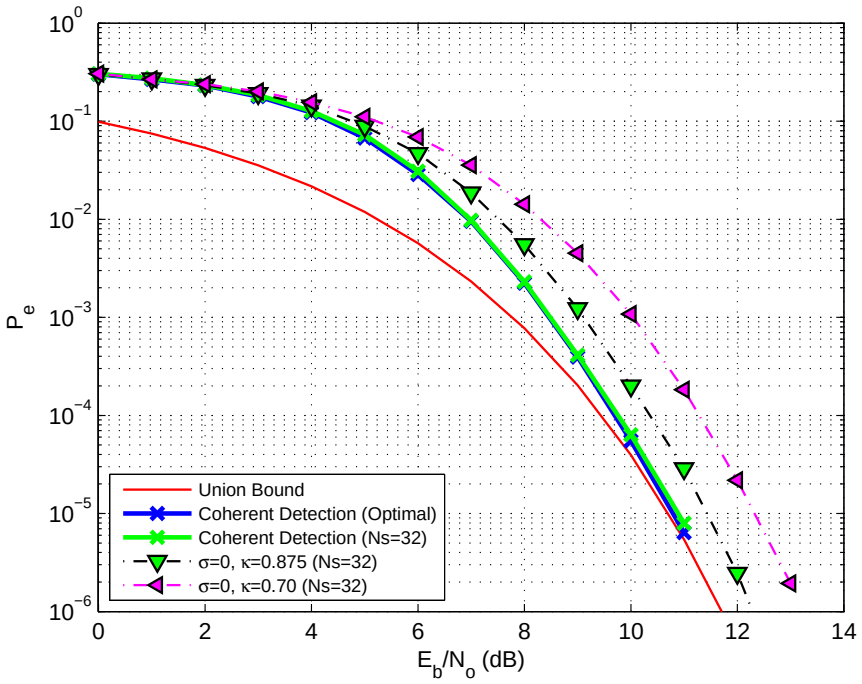

Figure 5.24. 32 state Non-Coherent ARTM CPM (Uncoded): $\sigma = 0°$/sym.

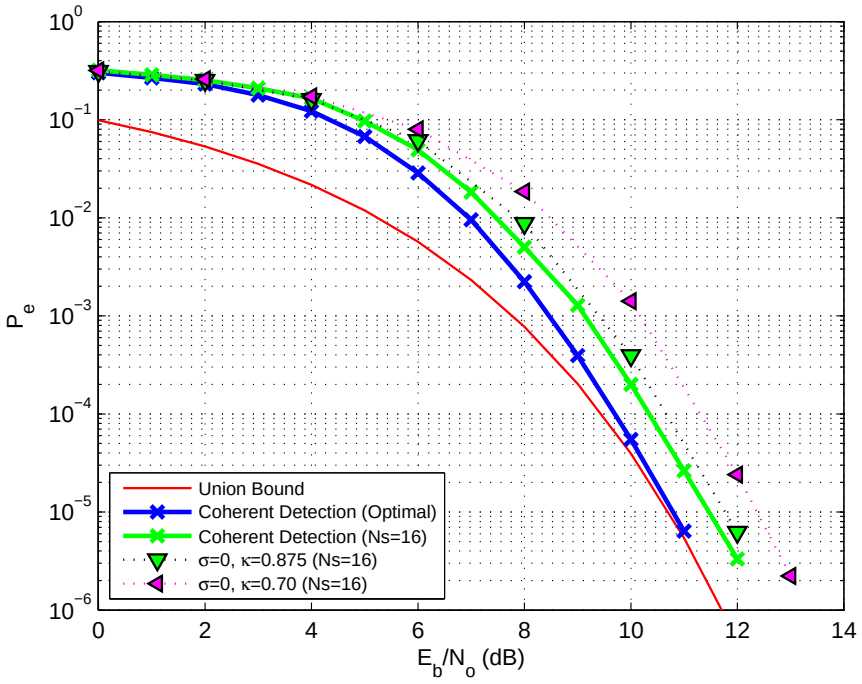

Figure 5.25. 16 state Non-Coherent ARTM CPM (Uncoded): $\sigma = 0°$/sym.

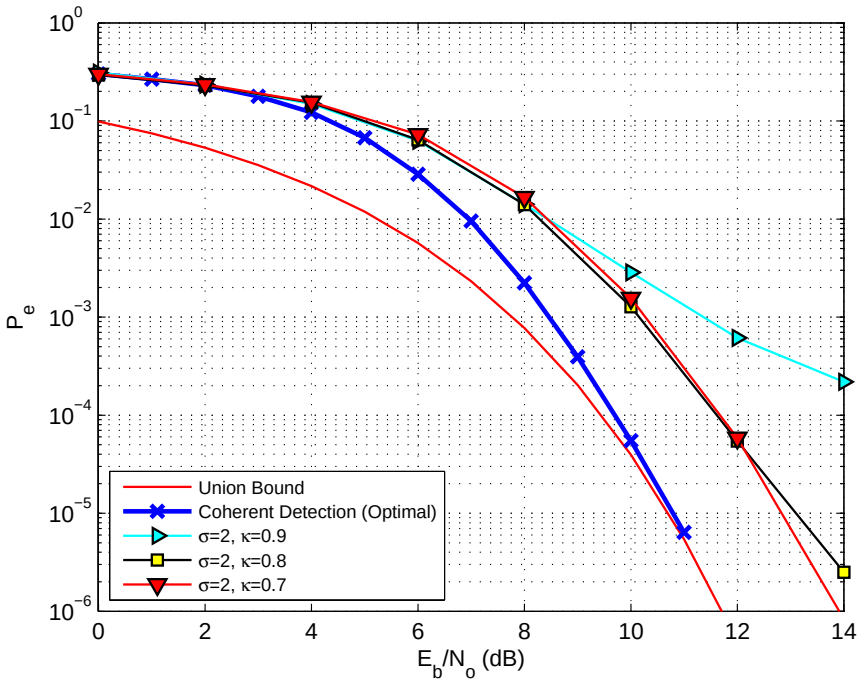

Figure 5.26. Non-Coherent ARTM CPM (Uncoded): $\sigma = 2^{\circ}$/sym.

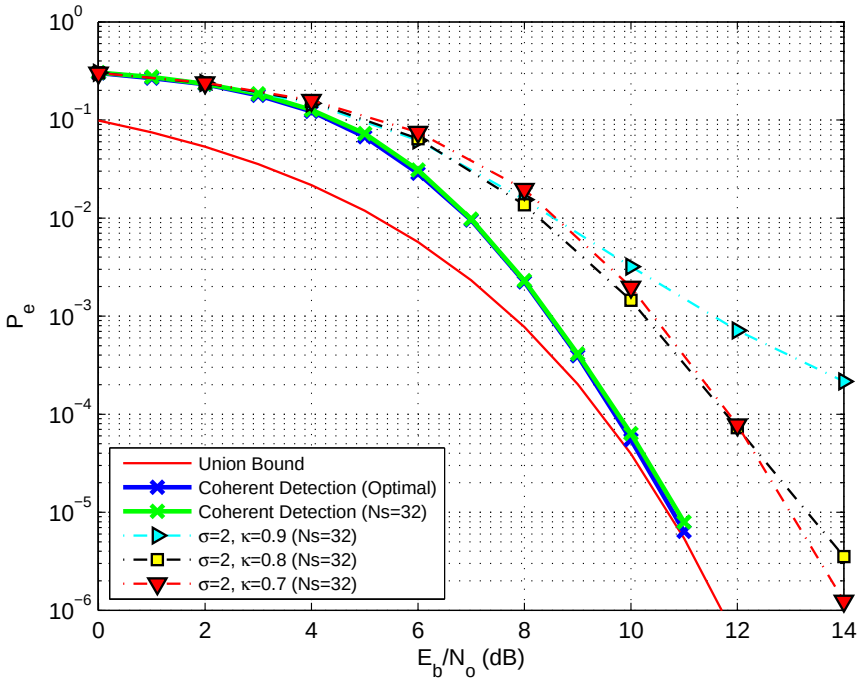

Figure 5.27. 32 state Non-Coherent ARTM CPM (Uncoded): $\sigma = 2^{\circ}$/sym.

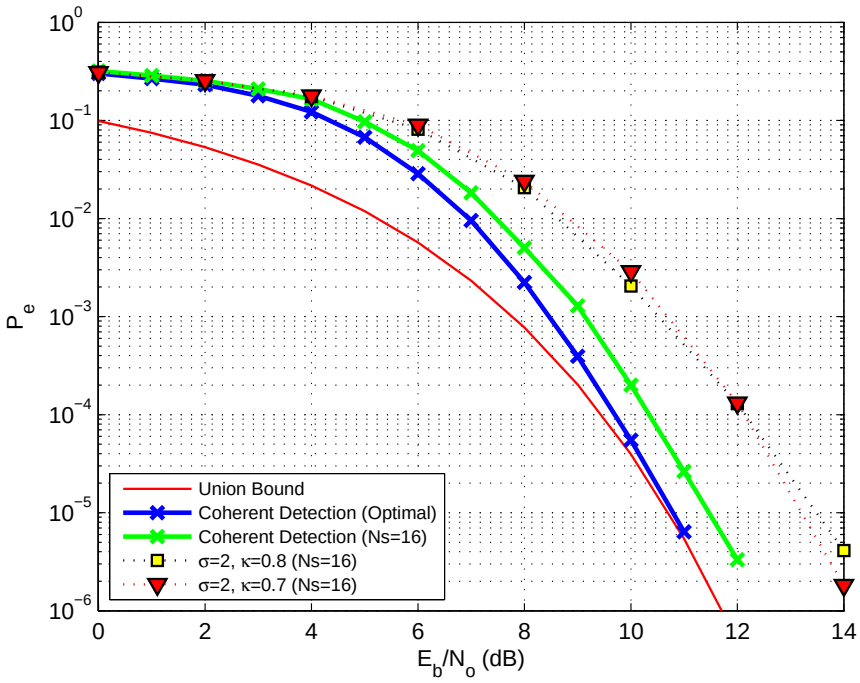

Figure 5.28. 16 state Non-Coherent ARTM CPM (Uncoded): $\sigma = 2°$/sym.

Case	*Phase Noise:* σ *(std.dev)*	*Loss in dB Uncoded*
1	$0°$	0.55
2	$2°$	2.04

Table 5.6. Non-Coherent Detection of ARTM CPM.

Chapter 6

Conclusions

6.1 Key Contributions

1. An SCC PCM/FM system was developed. Optimal (full state) decoding of PCM/FM in this system gives a coding gain of more than 6.5 dB over uncoded PCM/FM, with the use of 2048 interleaver and 5 iterations as shown in Fig. 5.2 and Fig. 5.1. This system gives a higher coding gain than the SOQPSK-TG detector presented in [6].

2. While optimal decoding of uncoded PCM/FM requires a decoder state complexity of 20 states, a 10 state detector with 0.01 dB performance loss and an 8 state detector with and 0.07 dB ($P_r = 8, L_r = 1$) loss were proposed (see Fig. 5.3, Fig. 5.4 and Fig. 5.5). The 10 state detector for SCC PCM/FM performs with just 0.02 dB loss and the 8 state SCC PCM/FM detector performs within 0.2 dB of the optimal state detector. The 8 state detector for SCC PCM/FM is better than the optimal SOQPSK-TG detector presented in [6] by nearly 0.5 dB.

3. In the case of uncoded ARTM, a 32 state detector ($P_r = 8, L_r = 2$) with *one-eighth* complexity and 0.1dB loss and a 16 state detector ($P_r = 4, L_r = 2$) with *one-sixteenth* complexity and 0.68dB loss are presented (see Fig. 5.6).

4. Non-coherent detectors were presented for uncoded PCM/FM, SOQPSK-TG and uncoded ARTM CPM. Motivated by high gains achieved by the coherent SCC systems, non-coherent detectors for SCC PCM/FM and SCC SOQPSK-TG are developed here for the first time using the proposed algorithm in Chapter 4. Performance of the non-coherent detectors under phase noise is studied. In the uncoded case, the detectors for PCM/FM, SOQPSK-TG (PT) [1] and ARTM CPM have a performance loss of 0.15 dB, 2.07 dB and 2.04 dB respectively. And in the coded case, the non-coherent detectors for PCM/FM and pulse truncated SOQPSK-TG have a loss of 0.35 dB and 0.71 dB respectively, which is a small amount of extra signal power needed to build simple, robust and compact receivers, without the use of PLLs.

5. The discussed reduced complexity techniques were combined with non-coherent detection in phase noise environments. A 10 state non-coherent detector for SCC PCM/FM is proposed ($P_r = 10, L_r = 1$), which performs within 0.04 dB of the full state non-coherent detector (see Fig. 5.12). In otherwords, the overall performance loss due to phase noise, lack of carrier phase recovery system (PLL) and reduced complexity approximation is $0.35{+}0.04{=}0.39$ dB relative to the optimal coherent detection. Secondly, a 16 state ARTM CPM non-coherent detector is presented, which is just 0.37 dB worse than the full state (256) non-coherent detector, under the same phase noise conditions (standard deviation of 2°/symbol).

[1] Pulse truncated SOQPSK-TG is considered in all the simulations.

This means an overall additional expense of signal power is limited to about 2.4 dB (compare Fig. 5.26 and Fig. 5.28).

6.2 Future Study

On the lines of SCC SOQPSK and SCC PCM/FM, SCC ARTM system could be built. Since ARTM is a quaternary CPM, the SISO algorithm for rate $\frac{1}{2}$ convolutional codes could be used to compute the needed code word probabilities instead of bit probabilities, which are the same as symbol probabilities for the CPM. In such a case, we are looking at a *symbol interleaved* SCC CPM system [19]. Similar to the 10 state SCC PCM/FM detector, reduced complexity SCC ARTM detectors could be built. Some initial work in this direction has already been done.

Appendix A

The choice of a CPM for a given application is guided by mainly 3 factors — detection efficiency, spectral efficiency and decoding complexity. In the following sections, each of the properties is highlighted.

A.1 Comparison of Power (Detection) Efficiencies

The BER performance of OQPSK and several CPMs is presented in Fig. 1. PCM/FM has the highest detection efficiency while ARTM CPM has the least detection efficiency. The BER union bounds for the modulations is given in Table 6.2, where

Case	*Modulation*	*Union Bound for* P_e
1	**PCM/FM** (Tier-0)	$Q\left(\sqrt{2.61\frac{E_b}{N_0}}\right)$
2	OQPSK	$Q\left(\sqrt{2\frac{E_b}{N_0}}\right)$
3	MSK	$2Q\left(\sqrt{2\frac{E_b}{N_0}}\right)$
4	SOQPSK-MIL [a]	$Q\left(\sqrt{2.36\frac{E_b}{N_0}}\right) + Q\left(\sqrt{1.73\frac{E_b}{N_0}}\right)$
5	**SOQPSK-TG** (Tier-1)	$Q\left(\sqrt{2.59\frac{E_b}{N_0}}\right) + Q\left(\sqrt{1.60\frac{E_b}{N_0}}\right)$
6	**ARTM** (Tier-2)	$\frac{15}{128}Q\left(\sqrt{1.29\frac{E_b}{N_0}}\right) + \frac{108}{128}Q\left(\sqrt{1.66\frac{E_b}{N_0}}\right)$

[a] The union bounds for SOQPSK- MIL & TG assume *differential encoding.*

Table 1. Union bounds for BER.

$$Q(x) \triangleq \frac{1}{\sqrt{2\pi}} \int_x^\infty e^{\frac{-x^2}{2}} dx. \tag{1}$$

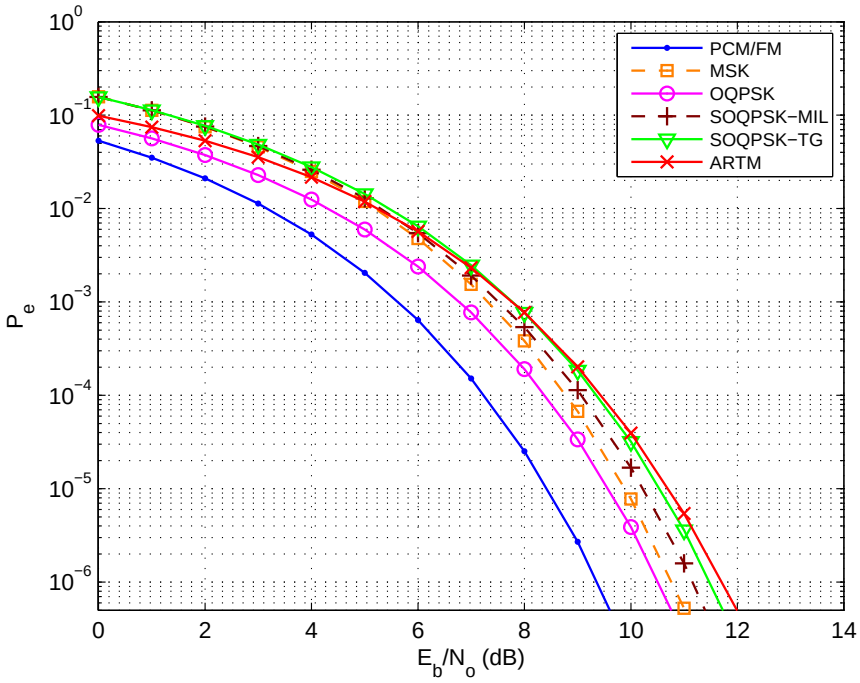

Figure 1. Comparison of BER Performances.

A.2 Comparison of Power Spectral Densities

A comparison of spectral efficiencies of the aeronautical telemetry CPMs against QPSK is shown in Fig. 2.

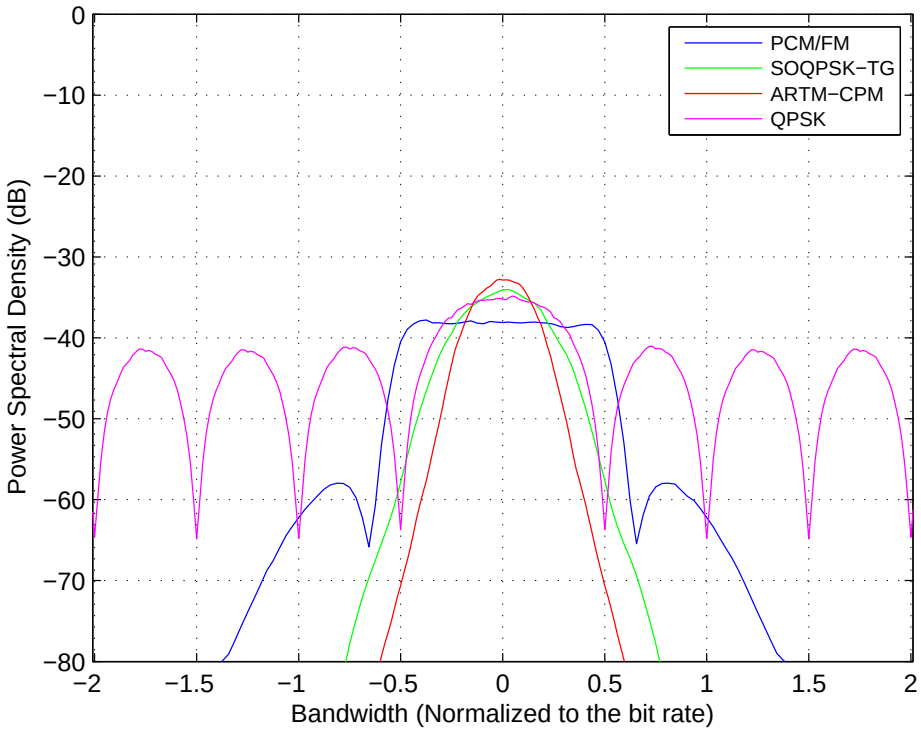

Figure 2. Comparison of Power Spectral Densities.

A.3 Comparison of Decoding Complexities

A comparison of decoding complexities for the aeronautical telemetry CPMs is presented in Table 6.2.

Case	*Modulation*	h	M	L	*Pulse Type*	*Number of States*	*Comments*
1	**PCM/FM** (Tier-0)	$\frac{7}{10}$	2	2	RC	20	*Regular CPM*
2	MSK	$\frac{1}{2}$	2	1	REC	2	*Regular CPM*
3	SOQPSK-MIL	$\frac{1}{2}$	2	1	REC	4	*Uses precoder* [a]
4	**SOQPSK-TG** (Tier-1)	$\frac{1}{2}$	2	8	TG	512	*Uses precoder*
5	**ARTM** (Tier-2)	$\frac{4}{16}, \frac{5}{16}$	4	3	RC	256	*Regular CPM*

Table 2. Comparison of CPM Parameters.

[a] Rimoldi's approach not considered for both versions of SOQPSK

Bibliography

[1] G. Ungerboeck, "Channel coding with multilevel/phase signals," *IEEE Transactions on Information Theory*, vol. 28, pp. 55–67, Jan. 1982.

[2] C. Berrou, A. Glavieux, and P. Thitimajshima, "Near shannon limit error-correcting coding and decoding: Turbo-codes," in *Proc. IEEE International Conference on Communications*, 1993.

[3] M. Simon, *Bandwidth-Efficient Digital Modulation With Application to Deep-Space Communication*. New York: Wiley, 2003.

[4] L. Lampe, R. Schober, and M. Jain, "Noncoherent sequence detection receiver for Bluetooth systems," *IEEE Journal on Selected Areas in Communication*, vol. 23, pp. 1718–1727, Sept. 2005.

[5] J. B. Anderson, T. Aulin, and C. E. Sundberg, *Digital Phase Modulation*. New York: Plenum Press, 1986.

[6] E. Perrins and M. Rice, "Reduced-complexity approach to iterative detection of SOQPSK," *IEEE Transactions on Communication*, vol. 55, pp. 1354–1362, July 2007.

[7] E. Perrins, R. Schober, M. Rice, and M. K. Simon, "Multiple-bit differential detection of shaped-offset QPSK," to be published in *IEEE Transactions on Communications*.

[8] P. Moqvist and T. Aulin, "Serially concatenated continuous phase modulation with iterative decoding," *IEEE Transactions on Communication*, vol. 49, pp. 1901–1915, Nov. 2001.

[9] T. Larsson, "Optimal design of CPM decoders based on state-space partitioning," in *Proc. IEEE International Conference on Communications*, (Geneva, Switzerland), pp. 123–127, May 1993.

[10] M. K. Howlader and X. Luo, "Noncoherent iterative demodulation and decoding of serially concatenated coded MSK," in *Proc. IEEE Global Telecommunications Conference*, vol. 2, pp. 785–789, Nov./Dec. 2004.

[11] L. Bahl, J. Cocke, F. Jelinek, and J. Raviv, "Optimal decoding of linear codes for minimizing symbol error rate," *IEEE Transactions on Information Theory*, vol. 20, pp. 284–287, Mar. 1974.

[12] S. Benedetto, D. Divsalar, G. Montorsi, and F. Pollara, "A soft-input soft-output APP module for iterative decoding of concatenated codes," *IEEE Communication Letter*, vol. 1, pp. 22–24, Jan. 1997.

[13] S. Benedetto, G. Montorsi, and D. Divsalar, "Concatenated convolutional codes with interleavers," *IEEE Communications*, vol. 41, pp. 102–109, Aug 2003.

[14] S. Benedetto and G. Montorsi, "Unveiling turbo codes: Some results on parallel concatenated coding schemes," *IEEE Transactions on Information Theory*, vol. 42, pp. 409–428, Mar. 1996.

[15] Range Commanders Council Telemetry Group, Range Commanders Council, White Sands Missile Range, New Mexico, *IRIG Standard 106-04: Telemetry Standards*, 2004. [Online]. Available: http://jcs.mil/RCC/manuals/106-04.

[16] A. Svensson, C.-E. Sundberg, and T. Aulin, "A class of reduced-complexity Viterbi detectors for partial response continuous phase modulation," *IEEE Transactions on Communication*, vol. 32, pp. 1079–1087, Oct. 1984.

[17] E. Perrins and M. Rice, "Reduced complexity detectors for multi-h CPM in aeronautical telemetry," *IEEE Transactions on Aerospace and Electronic Systems*, vol. 43, pp. 286–300, Jan. 2007.

[18] B. E. Rimoldi, "A decomposition approach to CPM," *IEEE Transactions on Information Theory*, vol. 34, pp. 260–270, Mar. 1988.

[19] M. Xiao, *Some Concatenated and Iterative Decoding Approaches for Continuous Phase Modulation*. Ph.D. dissertation, Chamlers University of Technology, Göteborg, Sweden, Dec. 2004.

[20] G. Colavolpe, G. Ferrari, and R. Raheli, "Noncoherent iterative (turbo) decoding," *IEEE Transactions on Communication*, vol. 48, pp. 1488–1498, Sept. 2000.

[21] G. Colavolpe and R. Raheli, "On noncoherent sequence detection of continuous phase modulations," *IEEE International Conference on Universal Personal Communications, 1998. (ICUPC '98).*, vol. 2, pp. 1111–1115, Oct. 1998.

[22] G. Colavolpe, G. Ferrari, and R. Raheli, "Reduced-state BCJR-type algorithms," *IEEE J. Select. Areas Commun.*, vol. 19, pp. 848–859, May 2001.

[23] R. Schober and W. H. Gerstacker, "Metric for noncoherent sequence estimation," *Electronic Letters*, vol. 35, pp. 2178–2179, Dec. 1999.